




Research Article

Characterization of spherical Ag nanoparticles synthesized from the agricultural wastes of *Garcinia mangostana* and *Nephelium lappaceum* and their applications as a photo catalyzer and fluorescence quencher

Kulathunga Mudalige Kalani Gayanthika Perera¹ · Kuruppu Arachchige Shashika Shehani Kuruppu¹ · Adikarie Mudiyanseelage Ruhunu Chamara¹ · Gobika Thiripuranathar¹ 

Received: 13 June 2020 / Accepted: 7 October 2020 / Published online: 10 November 2020
© Springer Nature Switzerland AG 2020

Abstract

The present investigation reports a comparative study of direct Sunlight and UV irradiation driven silver nanoparticles (AgNPs) synthesized from water extracts of seasonal fruit wastes of *Garcinia mangostana* L. (fruit rind and seed), and *Nephelium lappaceum* L. (peel and seed). Synthesized NPs were characterized using Ultraviolet–Visible spectrophotometry, Fourier Transform Infrared spectroscopy (FTIR), Scanning Electron Microscopy (SEM), Transmission electron microscopy (TEM), and Energy-dispersive spectroscopy (EDX). As per the SEM and TEM images, synthesized NPs appeared to be spherical, with a UV absorbance range of 400–440 nm. FTIR spectra demonstrated peaks at 3268–3290 cm^{-1} , 2347–2363 cm^{-1} , 2099–2103 cm^{-1} , and 1635–1639 cm^{-1} for fruit waste extracts, with low intensity for AgNPs. The particle size of AgNPs vary from 12.1–31.3 nm, as observed from the TEM, and the EDX spectra confirmed the purity of the AgNPs. The quenching ability of biogenic AgNPs was evaluated using Rhodamine B dye under Fluorescence spectrophotometry. As per the results, all biogenic AgNPs behaved as quenchers. The highest fluorescence quenching activity was observed in AgNPs synthesized via *G. mangostana* peel extract and *N. lappaceum* seed extract. The photocatalytic activity of the NPs was measured by the degradation of Methylene Blue dye under Sunlight. Among all four, AgNPs synthesized via *N. lappaceum* seed extract act as an effective photocatalyst, and the degradation efficiency was recorded as 95% with 22 min of Half-life. Thus, this study proposes that the synthesized biogenic AgNPs behave as an ideal material for dye degradation and fluorescence quenching.

Keywords Green synthesis · Agricultural waste · Nanoparticles · Photocatalytic · Fluorescence quenching

1 Introduction

Investigation and synthesis of nanoparticles (NPs) via eco-friendly materials in the form of whole cells, metabolites, or extracts from plants are gaining more popularity in nanoscience [1, 2]. Compared to other methodologies,

green synthesis has some distinct advantages and therefore being used to synthesize various metal NPs. This is mainly due to the high usage of chemicals or different energy forms in conventional methods, which leads to a negative impact on the environment [3–6]. Published scientific literature suggests that fabricated NPs can be used

Electronic supplementary material The online version of this article (<https://doi.org/10.1007/s42452-020-03640-y>) contains supplementary material, which is available to authorized users.

✉ Gobika Thiripuranathar, tgobika@ichemc.edu.lk | ¹College of Chemical Sciences, Institute of Chemistry Ceylon, Rajagiriya 10107, Sri Lanka.



SN Applied Sciences (2020) 2:1974 | <https://doi.org/10.1007/s42452-020-03640-y>

in numerous biological and physicochemical applications, which is due to their specific size and morphology [6–12].

Among all the metallic NPs, AgNPs have a prime position due to their numerous unique properties, which alluded to many applications. The optical, catalytic, electrical, biological, and electrochemical properties can significantly affect in diverse areas such as food, medicine, environmental, textile, and catalytic applications [8, 13, 14].

Numerous types of plant wastes (Cocos nucifera coir, corn cob, fruit seeds and peels, wheat bran, rice bran, palm oil mill effluent, kola seed shell, kola pod, cocoa pod husk, and avocado fruit peel) have been used to synthesize various metal NPs [1, 15–17]. The usage of agro-wastes is an eco-friendly and sustainable route for the effective usage of plant waste [1, 18]. As per the published literature, agro wastes of *G. mangostana* L. (Mangosteen) and *N. lappaceum* L. (Rambutan) are rich in secondary metabolites; therefore, these plant extracts can be used as reducing, stabilizing, and capping agent to synthesize AgNPs [19].

Mangosteen (*G. mangostana* L.) is a fruit-bearing tree, found in South and Southeast Asian countries, including Sri Lanka. The tree is abundant in Kaluthara District, which is situated in the Western Province of Sri Lanka. The tree grows up to about 6–25 m in height, contains leathery round leaves, and has slightly acidic sweet-flavored fruits that are round in shape. These fruits turned to a deep red-dish-purple when entirely ripped [20]. Various plant parts (fruit, leaves, bark, stem, and roots) of *G. mangostana* are used in ethnomedical treatments and proven to have anti-effective properties including antioxidant, anti-inflammatory, antibacterial, and antiviral activities [20, 21].

Rambutan (*Nephelium lappaceum* L.) is a tropical fruit originated in South and Southeast Asia and now spreading as an agricultural crop in many countries, including Singapore, Australia, and South Africa [22]. This evergreen tree grows up to 12–20 m in height, contains dark green, oval-shaped leaves. The oval or ellipsoid shaped fruits, once fully ripened, would have a color of yellow to bright red depending on the variety [22]. The fruit can be separated into hairy peel (2–4 mm in thickness), palpable fleshy fruit, and single seed. *N. lappaceum* is used to produce consumer products, and the plant parts, including the fruit, have shown to possess numerous biological activities including antioxidant, anti-inflammatory, antimicrobial, and antiviral activities [16, 22–25].

Industrial wastage generated from production processes such as textile or pharmaceutical carries dyes that can cause environmental threats. As many compounds being used are aromatic, they are not readily decomposable, can last in water bodies, and cause enduring damage to aquatic nature and life [26, 27]. Therefore, water purification technologies have also been developed through

a range of chemical, physical and biological approaches, including coagulation, flocculation, filtration, precipitation, ion exchange, membrane filtration, adsorption strategies, biodegradation approaches, and catalytic mechanisms [13]. Photocatalysis plays a crucial role in these methods, as it splits organic contaminants into the simplest gaseous types without producing secondary pollutants [17, 28].

The majority of the photocatalysts are UV active; therefore, the UV lights are necessary for efficient oxidation of organic contaminants. Therefore, the photocatalyst process under both UV and visible light are attractive, cost-effective, and efficient, which can use for industrial effluent treatment plants [13, 29]. Methylene Blue (MB) is one such major organic contaminant of industrial effluents, and it is stable at acidic pH [26, 29, 30]. Moreover, MB is used in medical fields as a disinfectant and biological stain [31]. MB is a toxic substance at high concentrations and low pH [26]; hence, the present study is focused on evaluating the photocatalytic effect of AgNPs on MB dye.

Rhodamine B is a conjugated polymer which has been used with a wide range of applications as chemical and biochemical sensor devices since it has a high fluorescence quantum yield. Fluorescence quenching of Rhodamine B can be achieved by inducing its fluorophore with quencher molecules through various molecular interactions to decrease the quantum yield [32]. Hence, Rhodamine B was utilized as an indicator to monitor the quenching behavior of biogenic AgNPs.

AgNPs have been synthesized using different approaches such as traditional heating, ultrasonic, laser irradiation, γ irradiation, and microwave irradiation, which originated from top-down and bottom-up approaches. However, the techniques mentioned above trigger high temperatures, high pressure, and other harmful substances that cause contamination in the environment [33]. Further, the previous studies have used ethanolic plant extracts to synthesize AgNPs that maximize the usage of chemicals [34, 35]. Hence this study is focused on synthesizing rapid, one step, eco-friendly, and cost-effective greener NPs using water extracts.

In contrast to the published literature related to the plant extract mediated synthesis of AgNPs, this remains the first attempt in synthesizing AgNPs using agricultural wastes generated from the *G. mangostana* and *N. lappaceum* fruits catalyzed by direct Sunlight and by UV irradiation [19, 36, 37]. The principal objective of this research was to study the comparison of the shape and the size of the biogenic AgNPs synthesized by irradiating direct Sunlight and UV light. Considering the physical parameters, direct Sunlight irradiated biogenic AgNPs were used to evaluate for their fluorescence quenching efficacy on Rhodamine B and photocatalytic activity by MB degradation. During the literature survey, it was found that the

fluorescence quenching ability of biogenic AgNPs on Rhodamine B was under-explored. Therefore this study was carried out to evaluate the fluorescence efficacy of AgNPs on Rhodamine B. The lack of published literature regarding the details on the acidity or basicity of the reaction medium in which photocatalytic assays of biogenic AgNPs was also brought into attention.

2 Materials and methodology

2.1 Materials

Silver nitrate (purchased from Sigma-Aldrich, Anala R grade), Ethanol (purchased from BDH, Anala R grade), Sodium hydroxide pellet (purchased from Sigma-Aldrich, Anala R grade), Hydrochloric acid (purchased from Sigma-Aldrich, Anala R grade), Rhodamine B (purchased from Sigma-Aldrich), Methylene Blue (purchased from Sigma-Aldrich).

2.2 Sample collection and preparation of the extracts

Previously published methods were used with appropriate modification to prepare *G. mangostana* and *N. lappaceum* extracts [6, 38, 39]. The ripened fruits of the common variety of *G. mangostana* available in Kaluthara district were gathered from households. The *N. lappaceum* fruits were also collected in the same manner from the Colombo district. Ripened fruits were washed with normal water, and then the peel and seed of *N. lappaceum* and fruit rind and the seed of *G. mangostana* were separated with a sharp knife. The separated parts were washed with water, cut into small portions, and air-dried for 2 days in the shade. Plant extracts were prepared by placing 3.00 g (Analytical balance-RADWAG Wagi Electroniczne, AS-220. R2) of powdered plant material in a flask containing 300.0 mL of deionized water and heating for 10 min at 100 °C. The crude extracts were filtered using Whatman No. 1 filter paper to separate the plant material from the aqueous water extracts.

2.3 Synthesis of AgNPs

Prepared plant waste extracts were mixed with different concentration of silver nitrate (AgNO_3) solutions in different volume ratios, irradiated with direct Sunlight or Ultraviolet light [UV light, the distance between the reaction mixture and the UV lamp (Philips, E/70/2 HPW-125-W) – 5 cm] and kept in the dark. Based on the optimization results, a suitable time was identified to collect the NPs. Resulted reaction mixtures were centrifuged at

4500 rpm (GEMMYCO, PLC-036 h) for 15 min to precipitate the NPs. Then the AgNPs were washed with deionized water followed by Ethanol and oven-dried (Universal oven-UN 55) at 50 °C for 12 h.

AgNPs synthesis from *G. mangostana* peel extract: Preparation of AgNPs under direct Sunlight: Extract obtained from *G. mangostana* peel (MPE) was mixed with AgNO_3 solution (1 mM) in 2:5 volume ratio of plant extract to AgNO_3 . This reaction mixture was irradiated with direct Sunlight for 10 min and was kept in the dark for up to 3 h. Preparation of AgNPs under UV light: MPE was mixed with AgNO_3 solution (1 mM) in 2:5 volume ratio of plant extract to AgNO_3 solution and was irradiated under UV light for 60 min and then kept in the dark up to 24 h.

AgNPs synthesis from *G. mangostana* seed extract: Preparation of AgNPs under direct Sunlight: Extract obtained from *G. mangostana* seed (MSE) was subjected to centrifugation (4500 rpm for 15 min) followed by the addition of Ethanol to remove the pectin sedimentation. Isolated supernatant of MSE was collected and mixed with AgNO_3 solution (10 mM) in a 1:1 volume ratio of plant extract to AgNO_3 . This reaction mixture was irradiated with direct Sunlight for 10 min and was kept in the dark until 1 h. Preparation of AgNPs under UV light: MSE was mixed with AgNO_3 solution (10 mM) in a 1:1 volume ratio of plant extract to AgNO_3 solution and was irradiated with UV light for 30 min and then kept in the dark up to 1 h.

AgNPs synthesis from *N. lappaceum* peel extract: Preparation of AgNPs under direct Sunlight: Peel extract obtained from *N. lappaceum* (RPE) was mixed with AgNO_3 solution (5 mM) in 1:5 volume ratio of plant extract to AgNO_3 . This reaction mixture was irradiated under direct Sunlight for 10 min and was kept in the dark for up to 1 h. Preparation of AgNPs under UV light: RPE was mixed with AgNO_3 solution (5 mM) in a 1:5 volume ratio of plant extract to AgNO_3 . The mixture was irradiated under UV light for 60 min.

AgNPs synthesis from *N. lappaceum* seed extract: Preparation of AgNPs under direct Sunlight: Seed extract obtained from *N. lappaceum* (RSE) was subjected to centrifugation (4500 rpm for 15 min) followed by the addition of Ethanol to remove the pectin sedimentation. Isolated supernatant (RSE) was collected and mixed with the AgNO_3 solution (10 mM) in a 1:1 volume ratio of plant extract to the AgNO_3 solution. The obtained reaction mixture was irradiated under direct Sunlight for 30 min and was kept in the dark for up to 1 h. Preparation of AgNPs under UV light: RSE was mixed with AgNO_3 solution (10 mM) in a 1:1 volume ratio of plant extracts to AgNO_3 , irradiated under UV light for 120 min.

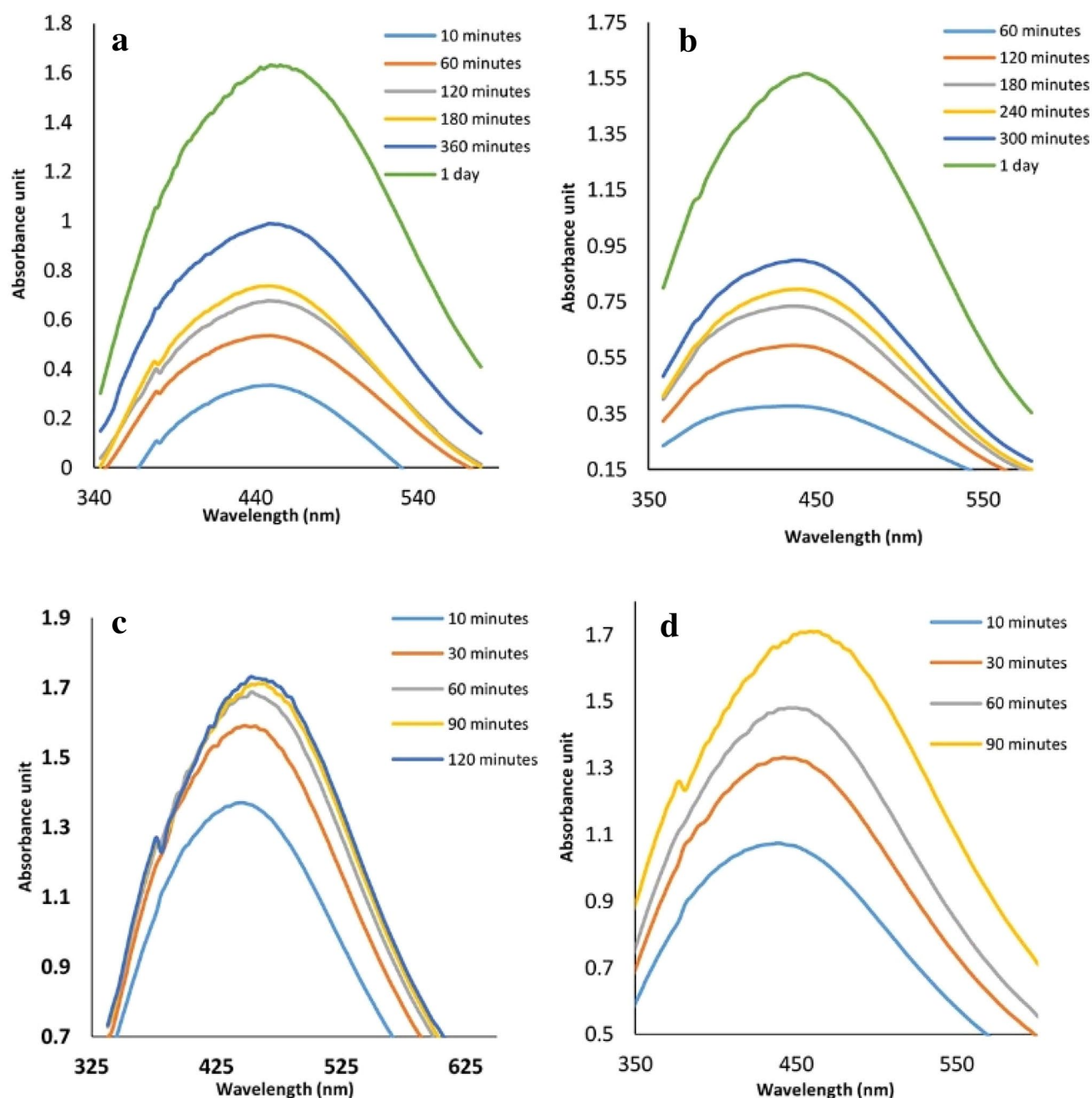


Fig. 1 UV-Visible spectra obtained for the synthesis of AgNPs using MPE **a** under sunlight **b** under UV light and MSE **c** under sunlight, **d** under UV light

2.4 Characterization of AgNPs

Ultraviolet-Visible spectroscopy (UV-VIS spectroscopy) (U-2910-Hitachi, Japan, and Vernier, Go Direct™ SpectroVis Plus) was used to monitor the fabrication of AgNPs. The synthesized NPs were further characterized by Fourier Transform Infrared spectroscopy (Horizon ABB-MB 3000 ATR FT-IR) (FTIR). The morphological features such as shape and particle diameter of NPs were characterized

by Scanning Electron Microscope (SEM) (Carl Zeiss, evo) and Transmission Electron Microscope (TEM) (JEOL JEM-2100 Japan) with Energy Dispersive Energy (EDX) system.

2.5 Fluorescence quenching ability of the synthesized AgNPs

The fluorescence quenching of Rhodamine B compound by the AgNPs was evaluated by fluorescence

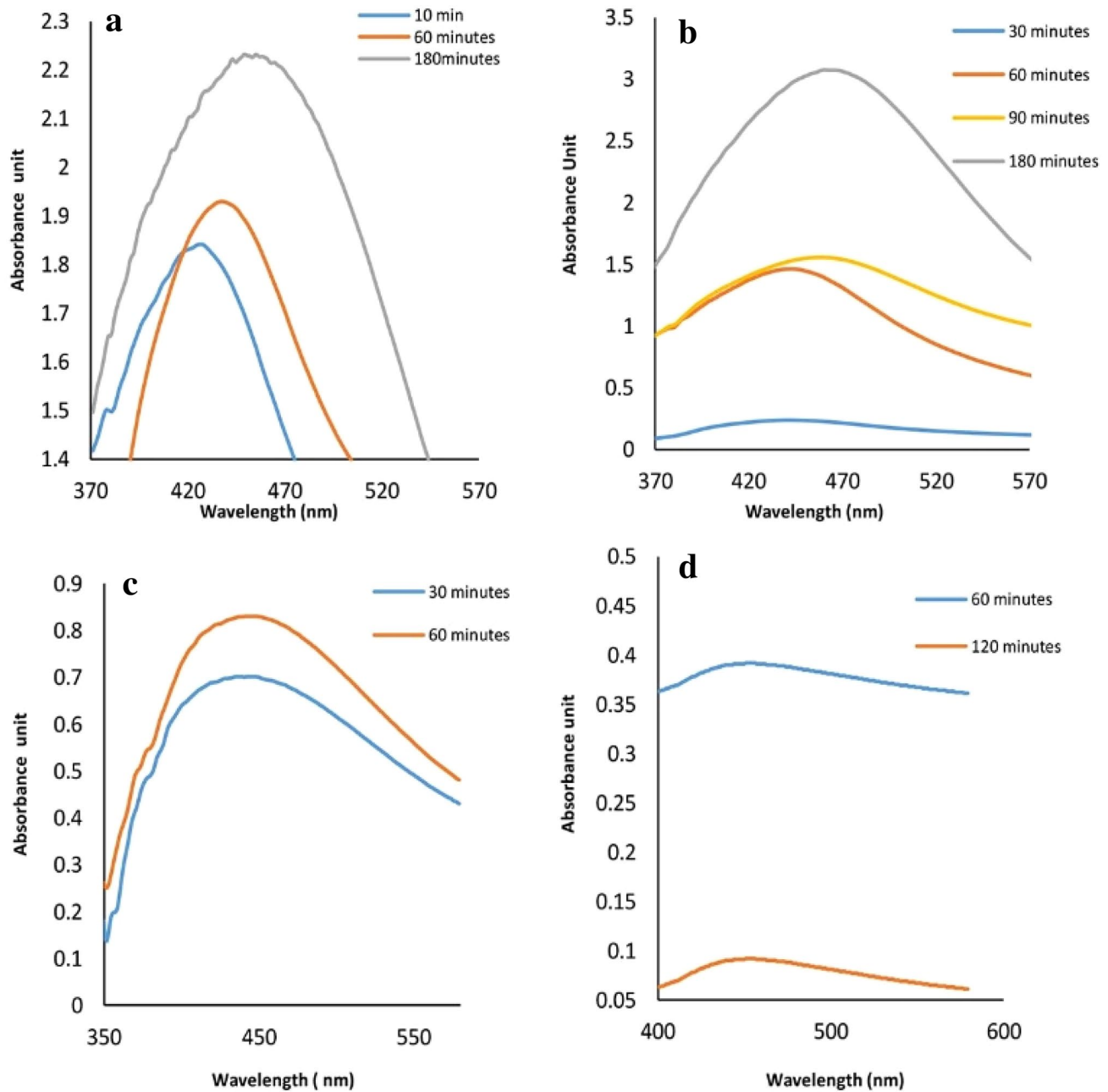
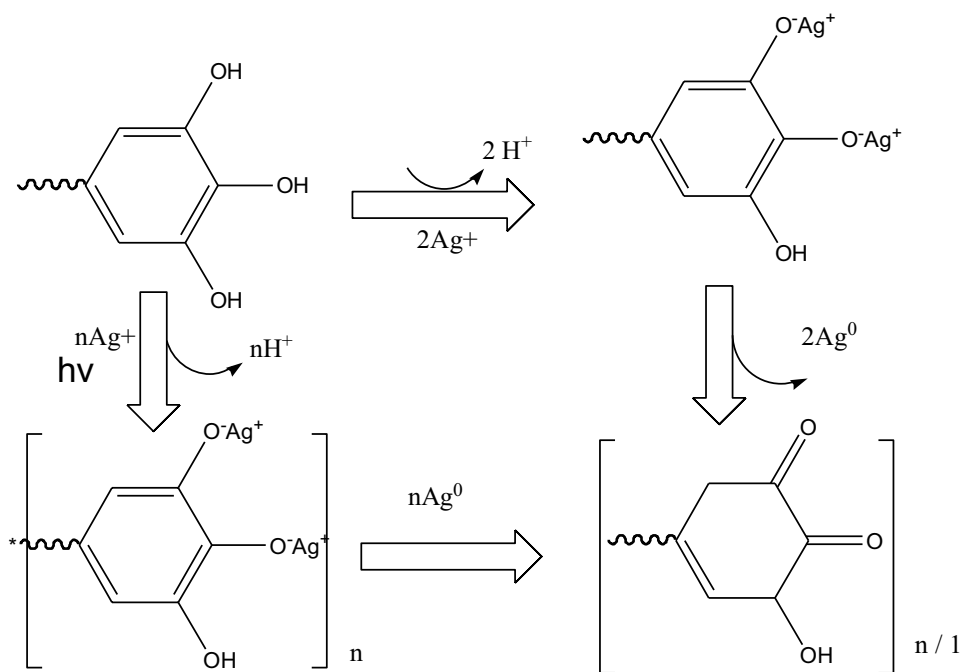


Fig. 2 UV-Visible spectra obtained for the synthesis of AgNPs using RPE **a** under sunlight **b** under UV light and RSE **c** under sunlight, **d** under UV light

spectrophotometry using a previously published method with appropriate modifications [40]. AgNPs synthesized under direct Sunlight irradiation were used to carry out the fluorescence quenching ability due to the yield and the particle size. A Rhodamine B solution (0.05 mM) was prepared in deionized water, and from the prepared solution, 1000 μL was treated with 50 μL , 100 μL , 250 μL , 500 μL , 750 μL , and 1000 μL volumes of AgNPs (0.2 mg/mL) in deionized water, synthesized using MPE, MSE, RPE, and

RSE. The solutions were topped up to 3000 μL with deionized water. The test samples were mixed by vortexing, and then the fluorescence intensity was recorded using Spectrofluorometer (F-2700 FL Hitachi, Japan).

Fig. 3 Proposed reaction mechanism for the AgNPs formation [56]



2.6 Photocatalytic activity of the synthesized AgNPs

Degradation of MB induced by direct Sunlight at different pH (pH 2, pH 6, and pH 10) in the presence of NPs was used to evaluate the photocatalytic activity of the synthesized AgNPs [41]. AgNPs synthesized by irradiating direct Sunlight was used to study the photocatalytic activity due to the yield and the particle size. Degradation of the MB at different pH: A pH study was carried out to evaluate the effect of the acidic/basic nature of the medium on the degradation of the dye. The initial pH of the MB was recorded (pH=6.53, GENWAY, 3510, benchtop meter). The pH of the MB was varied by adding 0.1 M HCl to make it acidic and by adding 0.1 M NaOH to alter it to basic. The prepared MB solutions at pH 2, 6, and 10 were kept under direct Sunlight, and the photocatalytic activity was recorded periodically. AgNPs (1.00 mg) were dispersed (Advance vortex mixture-VELP Scientifica ZX3) in 5.00 mL of distilled water. A 25.00 mL of MB solution (5 ppm, pH 2) was added into the prepared AgNPs solution. The reaction mixtures were placed under direct Sunlight (temperature of the environment: 35 ± 3 °C) with continuous stirring. Control was kept in the dark to monitor the activity in the absence of Sunlight. Degradation of the MB was monitored by withdrawing 3.00 mL aliquots from the reaction mixture at every 30-min interval, and UV–VIS absorbance was measured at 661 nm.

2.6.1 Adsorption isotherm study

The adsorption studies of MB were analyzed by varying the MB concentration (2.4 ppm, 2.8 ppm, 3.2 ppm, 3.6 ppm, 4.0 ppm) in the presence of a constant concentration of AgNPs (0.2 mg/mL) and by adjusting the pH to 2. UV–VIS spectrophotometer was used to measure the absorbance of the samples at 661 nm. Langmuir adsorption isotherm and Freundlich adsorption isotherm were plotted using the following equation. The below equation denote the amount of dye adsorbed per unit mass of adsorbent at equilibrium (q_e):

$$q_e \left(\frac{mg}{g} \right) = \left[C_0 \left(\frac{mg}{L} \right) - C_e \left(\frac{mg}{L} \right) \right] \times \frac{V(L)}{W(g)}$$

where C_0 is the initial concentration of MB (mg/L), C_e is the concentration of MB at equilibrium (mg/L), V is the volume of the solution (L), and W is the weight of the sorbent (g) [42, 43].

2.7 Statistical analysis

Means of three replicates and standard error ($SEr \pm$) were determined for all analysis obtained.

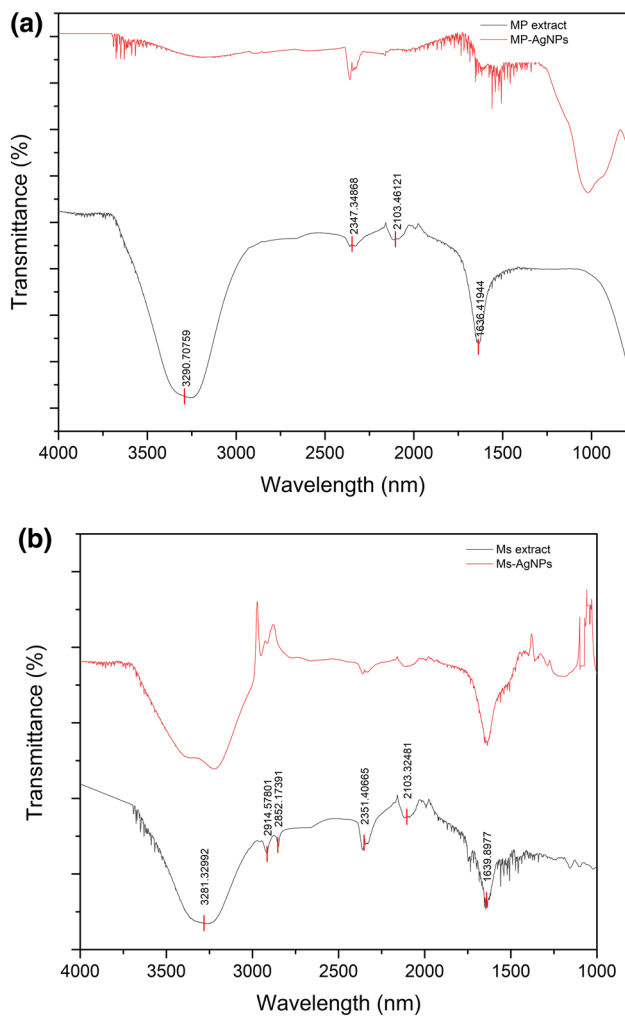


Fig. 4 FTIR spectra **a** MPE (in black) and AgNPs synthesized using MPE (in red) **b** MSE (in black) and AgNPs synthesized using MSE (in red)

3 Results and discussion

3.1 Synthesis and characterization of AgNPs

The synthesis of the AgNPs was optimized using different concentrations of AgNO_3 solution (0.8 mM, 1 mM, 2 mM, 2.5 mM, 3.0 mM, 5 mM and 10 mM) with using various plant extract to volume ratio and irradiation time of sunlight/UV light [38, 44]. During the optimization step, when the concentration of the AgNO_3 solution increases, the larger shift to the longer wavelength was observed in UV spectrometry due to the formation of larger AgNPs. For this study, the AgNO_3 concentration, 1 mM for MPE, 5 mM for RPE and 10 Mm for MSE and RSE was chosen by considering the stability, yield and the optimum wavelength of AgNPs.

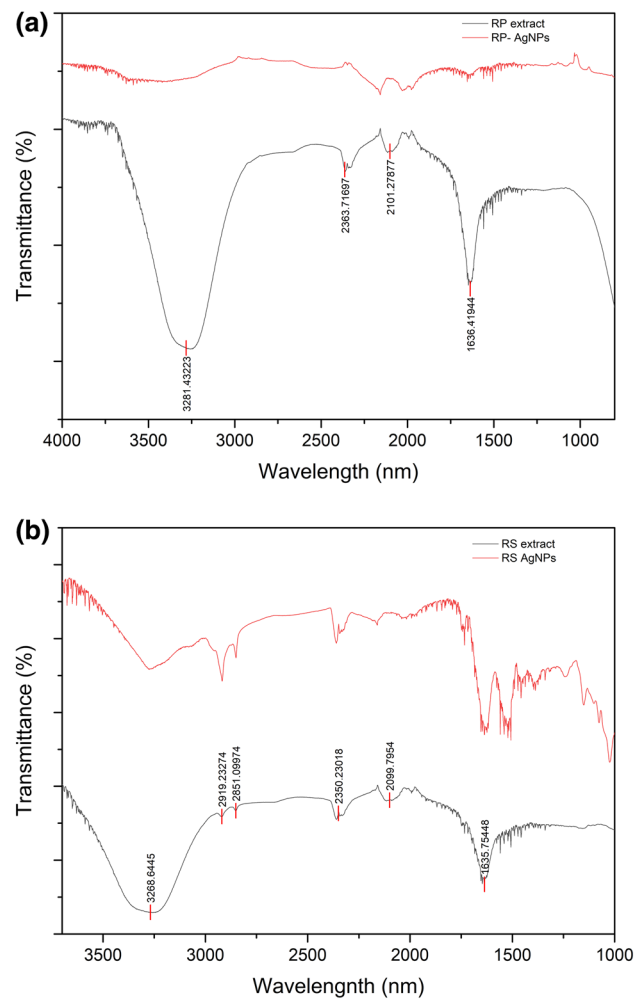


Fig. 5 FTIR spectra **a** RPE (in black) and AgNPs synthesized using RPE (in red) **b** RSE (in black) and AgNPs synthesized using RSE (in red)

UV–VIS Spectroscopy: One of the remarkable features of the metal NPs is their optical properties, which changes with the shape and the size [45, 46]. Dispersed metal NPs can be identified from the localized surface plasmon resonance (LSPR) phenomenon through UV–VIS Spectroscopy. [47]. The resonance frequency of localized surface plasmon of metallic NPs also depends on the shape, size, composition, and the degree of aggregation of metallic NPs [48]. Usually, the LSPR band of metallic NPs occurs in the UV range; however, in the case of Ag, the plasmon moves closer to the visible region due to the presence of electrons in the s atomic orbital. The AgNPs formation was confirmed by UV–VIS spectroscopy once the reaction medium changed its color from the initial color of light yellow to grey or dark red/orange color, which is due to the optical property of AgNPs [6].

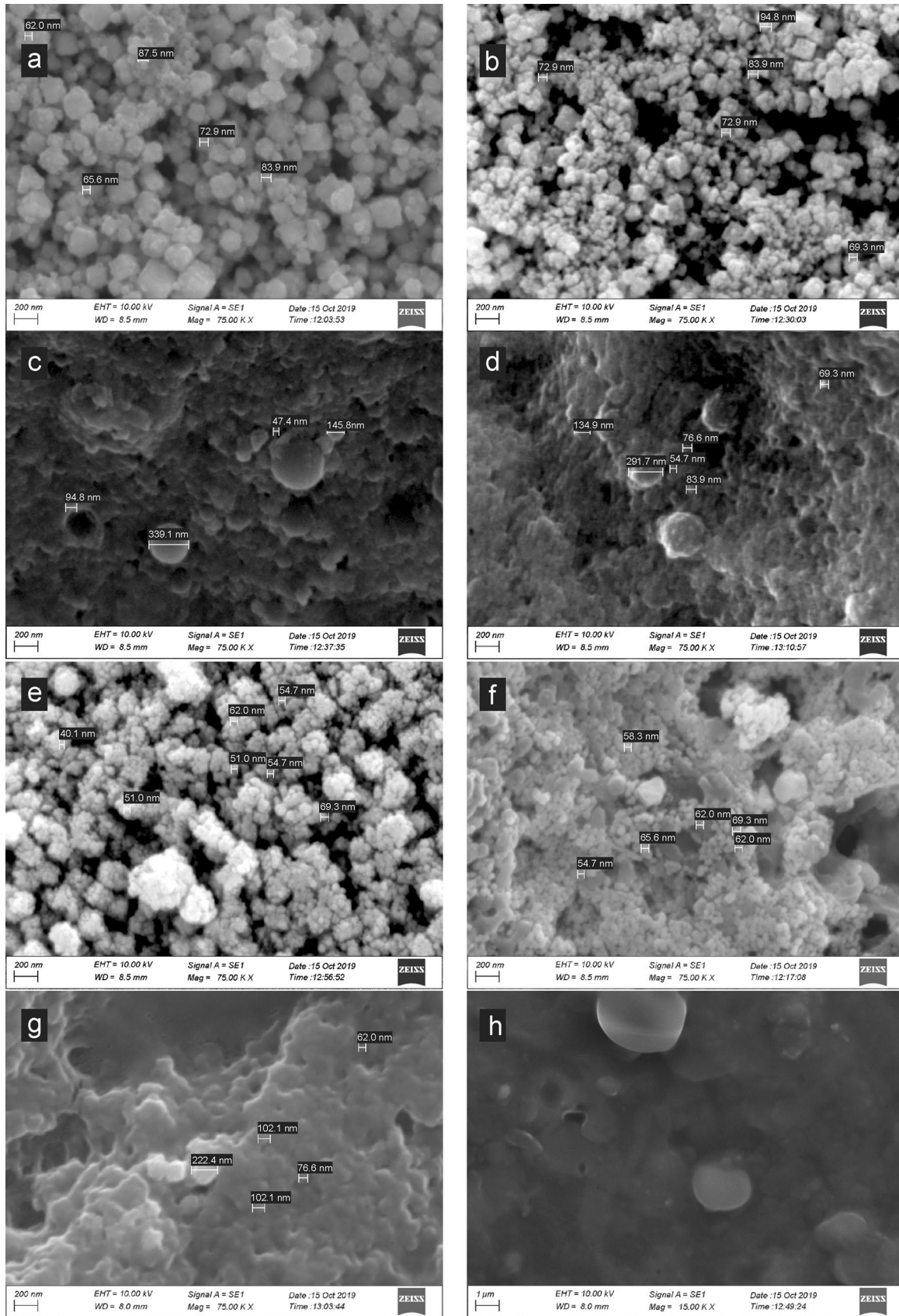


Fig. 6 SEM images of AgNPs synthesized via **a** MPE with sunlight treatment **b** MPE with UV light treatment **c** MSE with sunlight treatment **d** MSE with UV light treatment **e** RPE with sunlight treatment **f** RPE with UV light treatment **g** RSE with sunlight treatment **h** RSE with UV light treatment

During different time intervals (10 min–24 h), an aliquot of the reaction mixture was withdrawn to confirm the presence of AgNPs by UV–VIS spectroscopy. The synthesized AgNPs were within the range of 400–440 nm, as reported in the previous literature [38, 49, 50]. The wavelength of the NPs formed was considered in selecting optimum reaction time. UV light irradiation was carried out to evaluate the effect of UV light on the particle size and shape compared with the Sunlight irradiated samples. Figure 1a and b denote the UV–VIS absorbance spectra obtained for the synthesis of AgNPs using MPE under Sunlight and UV light, respectively. The (under Sunlight) wavelengths of the reaction mixture were recorded by periodical monitoring for up to 24 h as shown in Fig. 1a. The optimum reaction condition was identified as λ_{\max} 434 nm at 3 h, and therefore the AgNPs were collected at that time, which is in accordance with the published literature [51]. Figure 1b presents the UV–VIS absorbance spectra obtained for the synthesis of AgNPs with MPE under UV irradiation and wavelengths were monitored periodically for 24 h. were monitored periodically, as shown in the spectra. Even though the lowest λ_{\max} value was recorded at 408 nm after keeping under UV light for 60 min, the NPs were collected after 24 h due to the high yield.

Figure 1c and d represent the UV–VIS absorbance spectra for the synthesis of AgNPs using MSE under direct Sunlight and UV light, respectively. The NPs were collected at 420 nm due to the high yield for both Sunlight and UV irradiated MSE samples.

In Fig. 2a and b the UV–Visible absorbance spectra obtained for the synthesis of AgNPs from RPE under the direct Sunlight and UV light irradiations are given, respectively. Similar to NPs synthesized from MPE, considering the yield and the wavelength, the optimum time frame was identified. The λ_{\max} value obtained was in agreement with the published results [52]. Within a short period, a more significant shift to the longer wavelengths was observed for the direct Sunlight, as well as UV light irradiated samples, prepared by RPE compared to MPE.

Subsequent Fig. 2c and d provide the UV–VIS absorbance spectra obtained for AgNPs synthesized using RSE under direct Sunlight and UV light, respectively. Due to the considerable bathochromic shift, which changed the position of the spectral band to longer wavelengths, monitoring of the reaction time after 2 h period was ceased. The bathochromic shift of the spectrum is mainly due to the morphology and the size of the NPs [53]. Considering

the Sunlight mediated synthesis of NPs, UV light radiated synthesis took a longer time to initiate the reaction by changing the color.

3.2 Mechanism of formation of biogenic AgNPs

The present study experimented with the photoinduced synthesis of AgNPs utilizing the agro-waste of *G. mangostana* L. and *N. lappaceum* L. which was initiated by the absorption of photons (Sunlight and UV) by photosensitive biomolecules present in the plant extracts.

The high content of phytochemicals such as Alkaloids, Flavanoids, Triterpenoids, Terpenoids, Tannin, Saponin, Quinone, Protein, and Sugars are present in many plant extracts which are photosensitive [1, 15, 19]. Phytochemicals such as Flavonoids, Tannins, and many sugars act as reducing agents and while other phytochemicals act as capping or stabilizing agents in the process of synthesizing AgNPs.

Numerous polyphenolic compounds are present in *G. mangostana* L. and *N. lappaceum* L. plant extracts, which can be involved in many reduction pathways. The possibility of polyphenols or tannins to act as reductants is comparatively higher due to the prominent quantity of these chemicals in *G. mangostana* L. and *N. lappaceum* L. [54, 55]

The tannins molecules contain many –OH groups, which can get oxidized to quinoid form by donating electrons to Ag^+ to form Ag^0 . Many terpenols, flavin binding proteins, and most of the phytochemicals are photoreponsive; they either itself can donate the electrons or can induce other compounds to donate electrons to the Ag^+ in the presence of photons, which provides clear proof of photoinduced synthesis of AgNPs. Some alternative reducing reactions can also take place due to the reducing sugars present in the plant extracts. Whereas sugars, proteins, or some other phenolic compounds present in the plant extracts can behave as stabilizers for the synthesis of AgNPs [56, 57] (Fig. 3).

3.3 FTIR analysis of the plant extracts and synthesized AgNPs

Plant extracts contain many secondary metabolites that act as the reducing and capping agents in the green synthesis of metal NPs [6]. FTIR analysis was carried out in order to identify the functional groups present in the biomolecules which are responsible for the synthesis and stabilization of the synthesized AgNPs [58]. The FTIR spectra of the *N. lappaceum* and *G. mangostana* plant extracts were separately gathered as a means of identifying functional groups of the secondary metabolites in plant extracts that could contribute to the reduction of Ag^+ [51]. Infrared (IR) absorption of the AgNPs was arisen due to the

molecules that adhered to the surface of the NPs. A comparison between the plant extracts and the synthesized NPs could provide information on the surface adherence of molecules. Washing step with methanol could be a reason for the low intensity of IR peaks as this wash away the secondary metabolites adhering to the surfaces.

Table 1 Physical characteristics obtained from UV–VIS analysis and the SEM images

Plant extract	λ_{\max} value (nm)	Particle shape	Particle diameter (nm)
MPE—sunlight	434	Spherical	62.0–87.5
MPE—UV light	408	Spherical	69.3–94.8
MSE—sunlight	420	Spherical	47.4–95.1
MSE—UV light	420	Spherical	54.7–291.7
RPE—sunlight	433	Spherical	40.1–69.3
RPE—UV light	420	Spherical	54.7–69.3
RSE—sunlight	423	Spherical	65.6–113.3
RSE—UV light	415	Spherical	–

Particle sizes are given as observed by the SEM images

Figures 4 and 5, denote the FTIR spectra obtained for plant extracts, and AgNPs synthesized using the plant extract of MPE, MSE, RPE, and RSE, respectively. The common prominent peaks in all the spectra from plant extracts appeared in $3268\text{--}3290\text{ cm}^{-1}$, $2347\text{--}2363\text{ cm}^{-1}$, $2099\text{--}2103\text{ cm}^{-1}$ and $1635\text{--}1639\text{ cm}^{-1}$. These high-intensity peaks could be attributed to --OH vibration, --CN stretching, $\text{C}\equiv\text{C}$ stretching, and C=O stretching, respectively [8, 59, 60]. Peaks at $2914/2919\text{ cm}^{-1}$ and $2851/2852\text{ cm}^{-1}$ appeared in both the seed extracts, which correspond to the C--H vibration in the --CH_2 group. Seeds usually contain a high level of fatty acids/fatty acids like molecules in contrast to high flavonoid or phenolic compounds present in peel and edible portions. That could be mainly due to the CH_2 groups present in the seeds.

3.4 SEM analysis of the synthesized AgNPs

The physical characteristics of the synthesized AgNPs were evaluated through SEM. The analysis was carried

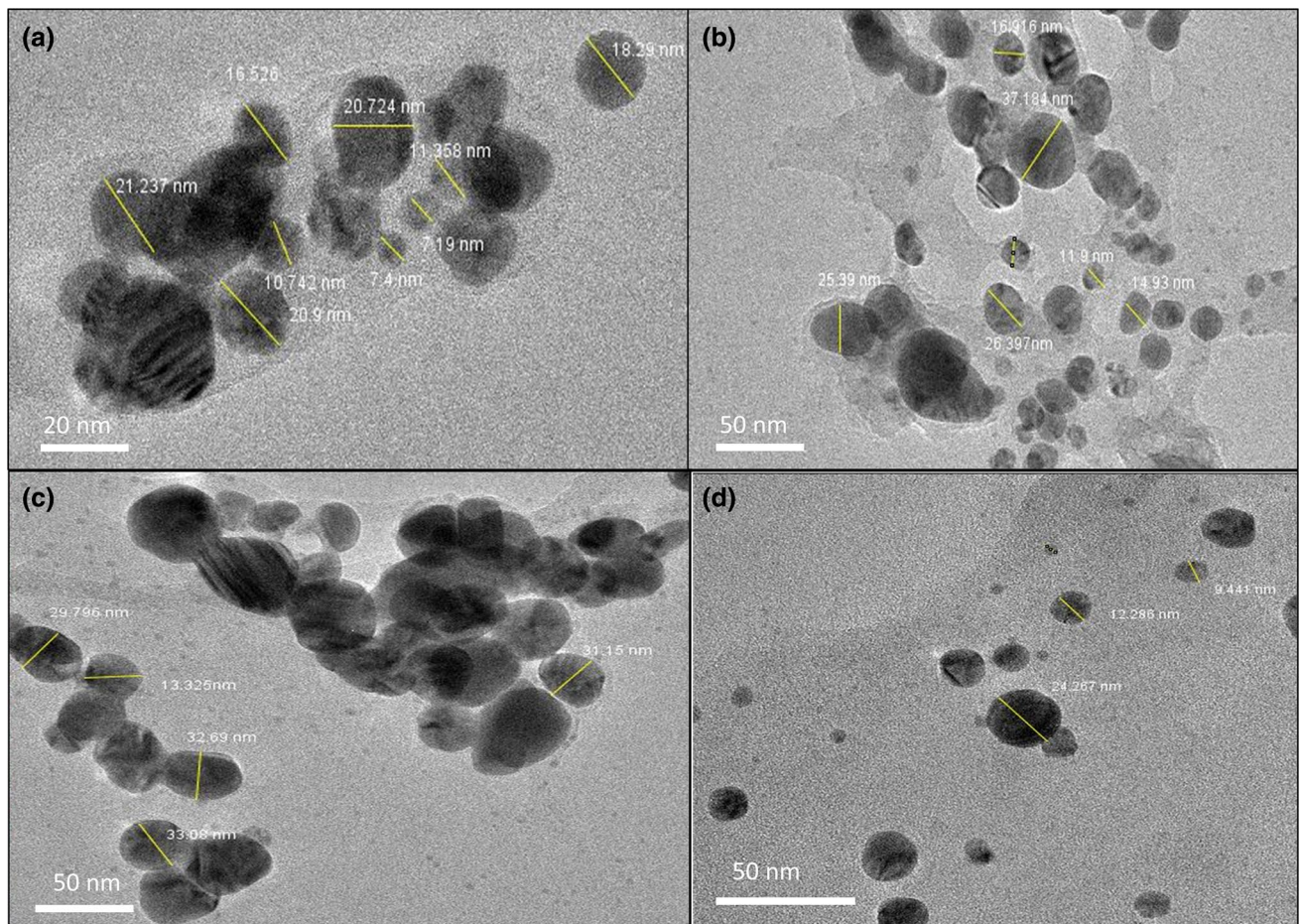


Fig. 7 TEM images of AgNPs synthesized via **a** MPE, **b** MSE, **c** RPE and **d** RSE

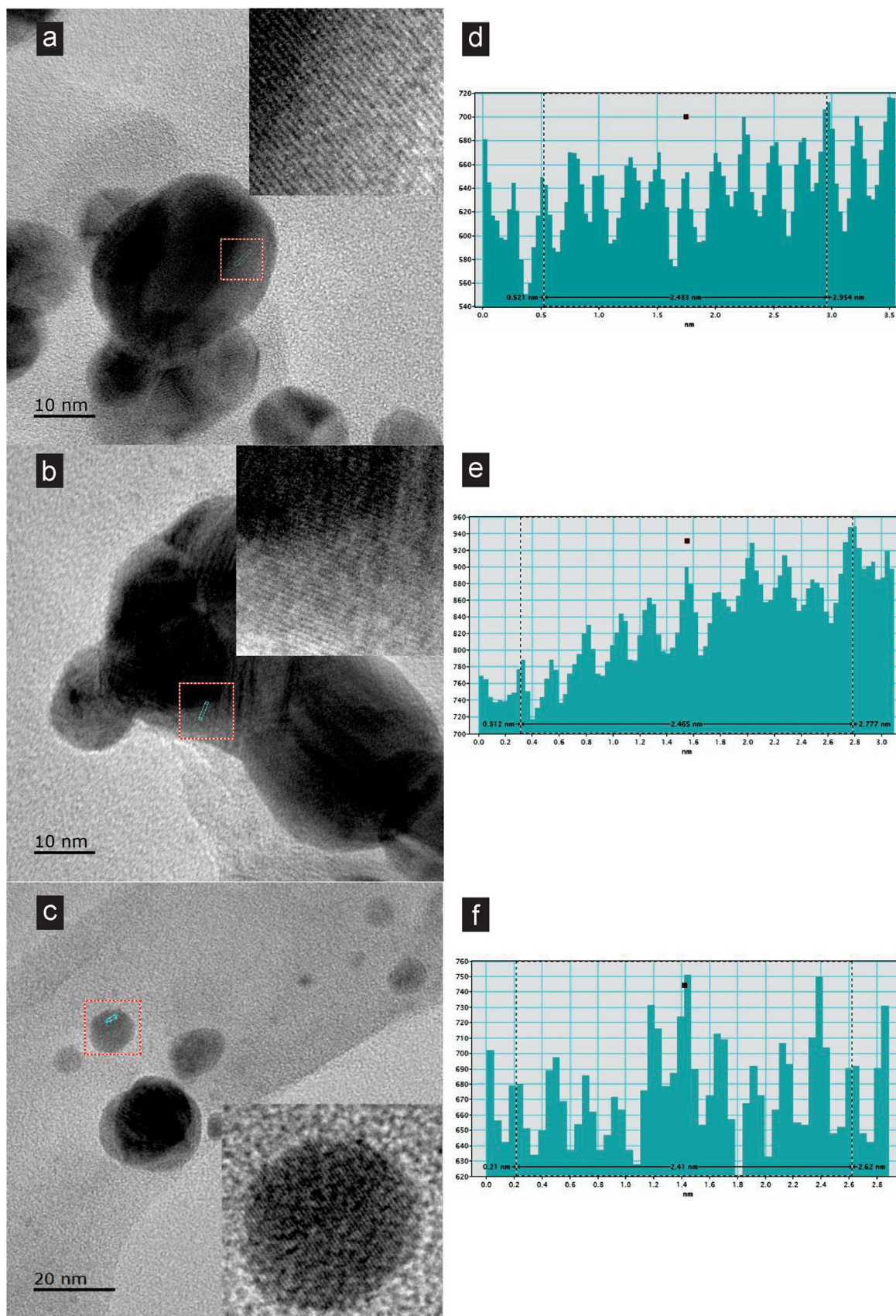
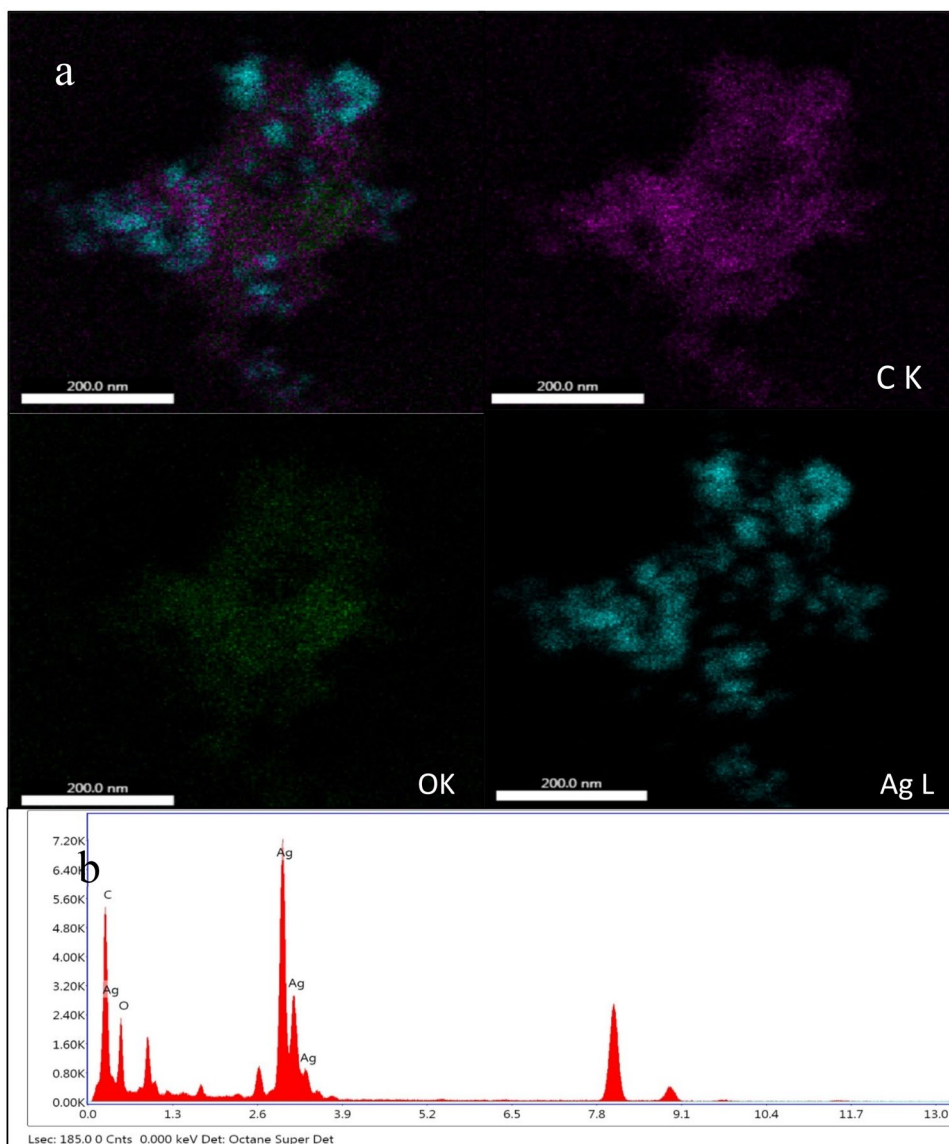


Fig. 8 TEM images of AgNPs Synthesized via **a** MPE, **b** MSE, **c** RSE and line profile of the HRTEM image of AgNPs synthesized via **d** MPE, **e** MSE, **f** RSE

Fig. 9 EDX **a** mapping and **b** spectrum of AgNPs synthesized via MPE



out in different magnitudes (15,000, 30,000, and 75,000) at 10 000 kV to investigate the particle shape and the size. AgNPs synthesized using MPE and RPE showed spherical particles which gathered in the form of clusters in both Sunlight and UV light treated samples, as shown in Fig. 6a, b, e and f. However, AgNPs obtained through seed extracts showed high agglomeration for both Sunlight and UV light treated samples that may be due to the high-fat content, as shown in Fig. 6c, d, g and h.

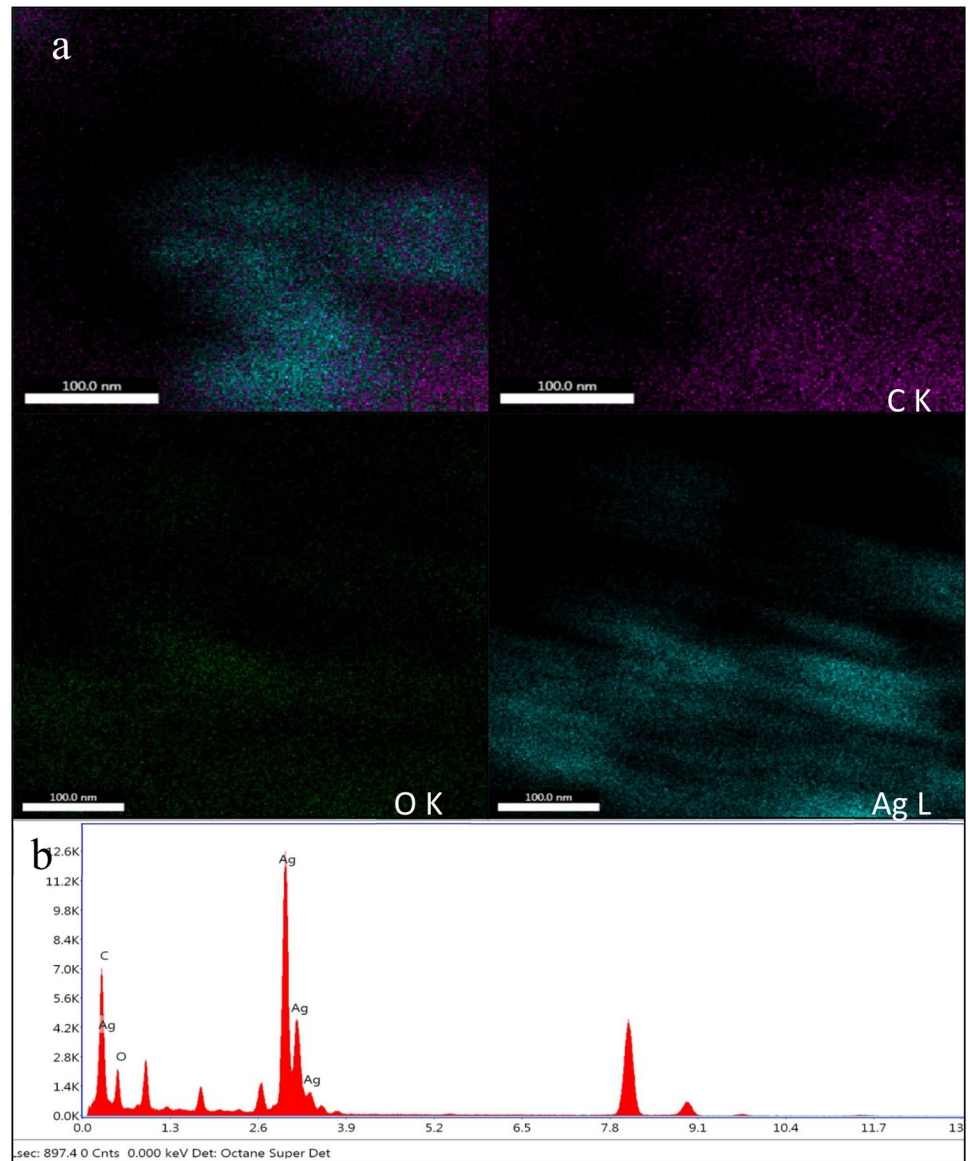
The information on NPs size was observed as given by the SEM images. The details obtained through UV–VIS spectroscopy and SEM are summarized in Table 1. By observing the UV–VIS spectra of the NPs and the SEM images, it can be concluded that Sunlight is far effective in the NPs fabrication process than the UV light irradiation. A possible reason may be the structural deformation and

loss of antioxidant activity that might occur in the secondary metabolites in the presence of UV light.

3.5 TEM and EDX analysis of the synthesized NPs

TEM analysis results depict that all the NPs were fallen within the nano range, and the NPs were approximately spherical, which also was confirmed by the SEM images. Figure 7 depicts the TEM images of the synthesized AgNPs via MPE (Fig. 7a), MSE (Fig. 7b), RPE (Fig. 7c), and RSE (Fig. 7d). The average diameter of the AgNPs synthesized via MPE, MSE, RPE and RSE were detailed as 14.9 ± 5.7 nm, 19.2 ± 7.2 nm, 31.3 ± 9.2 nm, and 12.1 ± 5.9 nm, respectively. Moreover, the TEM images revealed that the AgNPs synthesized from seed extracts had high agglomeration

Fig. 10 EDX **a** mapping and **b** spectrum of AgNPs synthesized via MSE



compared with the AgNPs synthesized via peel extracts, which was exhibited similarly in SEM images.

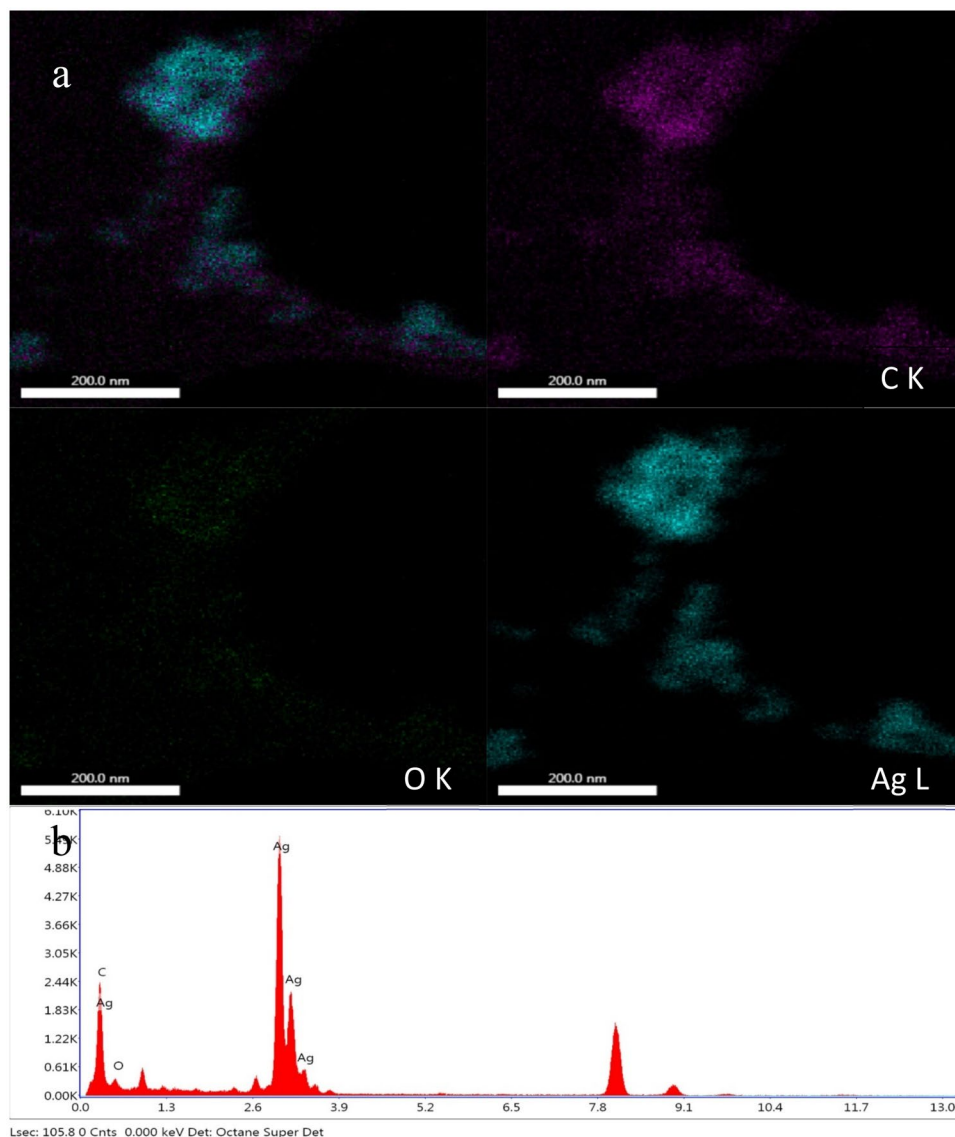
The results reported by Kumar et al. indicates that the NPs synthesized via *N. lappaceum* peel was fallen within the range of 132.6 ± 42 nm [19]. However, in this study, the AgNPs were synthesized successfully with an average particle size of 31.3 ± 9.2 nm. This variance may be due to the differences in the concentration of the plants or AgNO_3 and the radiation media used.

Atomic resolution cross-section of AgNPs synthesized via MPE, MSE, and RSE TEM image is given in Fig. 8d–f, respectively, which demonstrated the precise and uniform fringers. The atomic interlayer distance of all three AgNPs was estimated, and that was recorded as 0.24 nm, which

was closer to the lattice spacing of 0.232 of the (111) lattice planes of bulk Ag [61, 62].

The elemental composition of the AgNPs synthesized via MPE, MSE, RPE, and RSE was investigated by EDX analysis. The EDX spectrum illustrated (Figs. 9, 10, 11 and 12) that they have well-defined peaks related to Silver, Oxygen, and Carbon. The Carbon peak can be responsible for either to the biomolecules that are capped to the surface of AgNPs and/or to the coating of the copper grids. Besides, EDX spectra have shown the presence of extremely pure NPs without any other impurity-related peaks [63].

Fig. 11 EDX **a** mapping and **b** spectrum of AgNPs synthesized via RPE



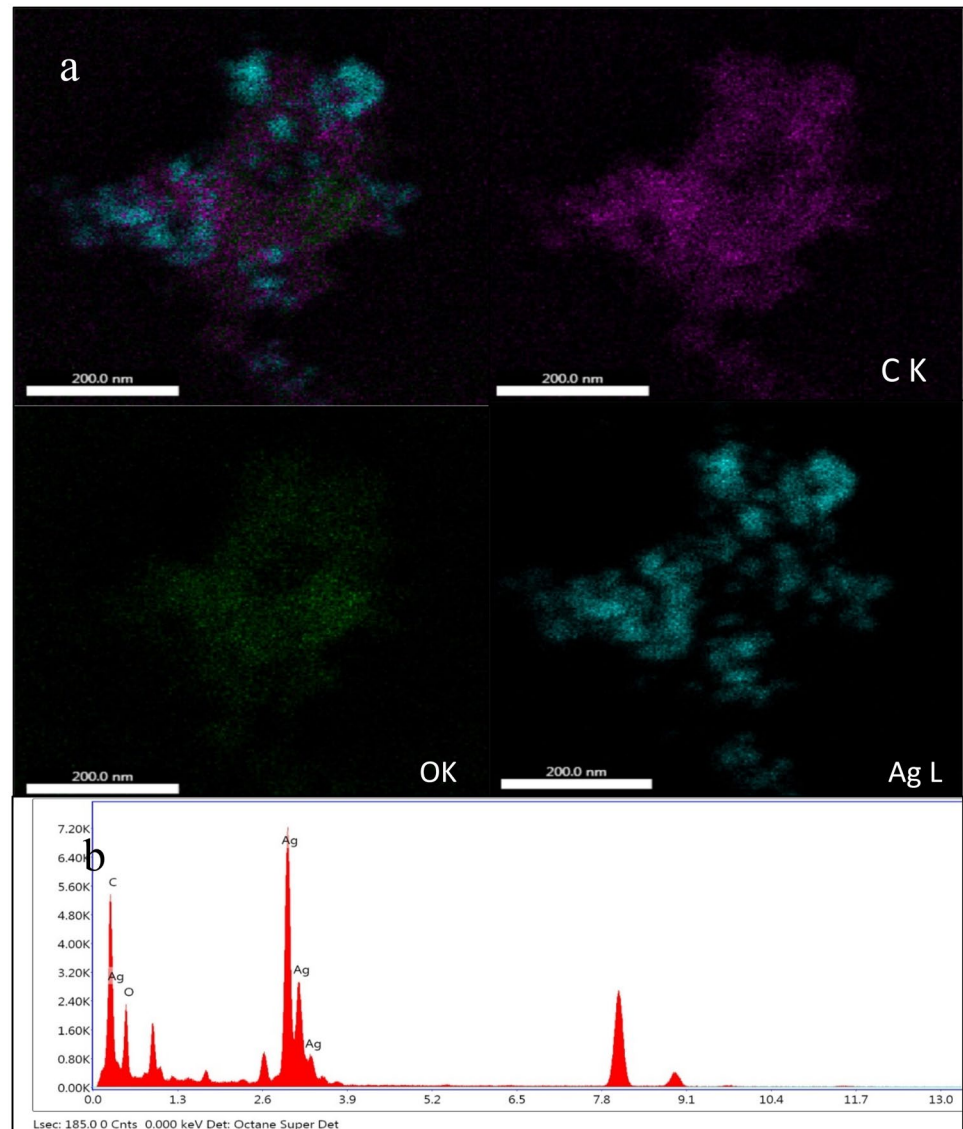
3.6 Fluorescence quenching activity of the synthesized AgNPs

The fluorescence quenching ability depends on the nature of fluorophore, quencher concentration, quencher molecule, and polarity of the solvent medium [64]. The fluorescence quenching efficacy of the synthesized NPs using MPE, MSE, RPE, and RSE dispersed in water was studied using fluorescence spectroscopy. Figure 13 summarizes the fluorescence emission spectra of Rhodamine B treated with AgNPs synthesized using MPE, MSE, RPE, and RSE, respectively. The spectral lines obtained for the fluorescence emission of Rhodamine B with AgNPs of each sample for 50 μ L, 100 μ L, 250 μ L, 500 μ L, 750 μ L, and 1000 μ L are given below. It was observed that in all the samples treated with AgNPs synthesized from MPE, MSE,

RPE, and RSE, the fluorescence intensity of the Rhodamine B decreased gradually with an increasing volume of the AgNPs solution. The use of green synthesized AgNPs as quencher molecules exhibit various advantages such as a cost-effective, eco-friendly, and easy process.

Fluorescence quenching can be due to either dynamic quenching or static quenching [40]. The Stern–Volmer equation is used to describe the dynamic quenching mechanism [40]. The data obtained through the fluorescence emission spectra were used to generate the Stern–Volmer plots for AgNPs treated with Rhodamine B is represented in Fig. 14. High linearity was observed for all the samples with $R^2 > 0.9596$. At the lower concentration, all four plots appeared to be linear, corresponding with the presence of a dynamic quenching mechanism. However, a positive deviation at higher concentration (0.035–0.07 M)

Fig. 12 EDX **a** mapping and **b** spectrum of AgNPs synthesized via RSE



was observed in the AgNPs synthesized via RPE, MSE, and RSE. In order to confirm this experimental observation, further studies have to be carried out with a narrow interval of concentrations. The reasons for deviation from the linearity may be due to the presence of dynamic and static quenching at the same time and also due to the formation of excited-state collisions or chemical complex [65, 66].

3.7 Photocatalytic activity of synthesized AgNPs

Various studies reported the catalytic effect of biofabricated nanomaterials in the process of reducing hazardous organic substances. Interestingly, AgNPs act as an efficient catalyst in the decolorization of dyes, which gives evidence that nanocatalyst has an industrial role due to high efficiency and reaction rate [67]. Hence, the present study has been carried out utilizing phytofabricated AgNPs via

agricultural wastes of *G. mangostana* and *N. lappaceum* for the degradation of MB.

When the photons irradiated to the AgNPs dispersed medium, the collective oscillations of electrons from the outermost band to a higher energy state take place. The plasmonic excitation of a surface electron is absorbed by molecular oxygen, which is present in the reaction medium, and it is converted into radical oxygen species. The positive charge generated in AgNPs (5 sp band) is filled with the electrons captured from the MB; thus, the MB dye adsorbed to the surface of the AgNPs. As a result, the MB dye gets oxidized. Meantime the hydrogen ions get generated from the reaction medium. The generated oxygen radical species willing to react with hydrogen ions and form hydroperoxyl radicals. The generated reactive radical species are responsible for the reduction of MB dye, and the proposed mechanism is given in Fig. 15 [68, 69].

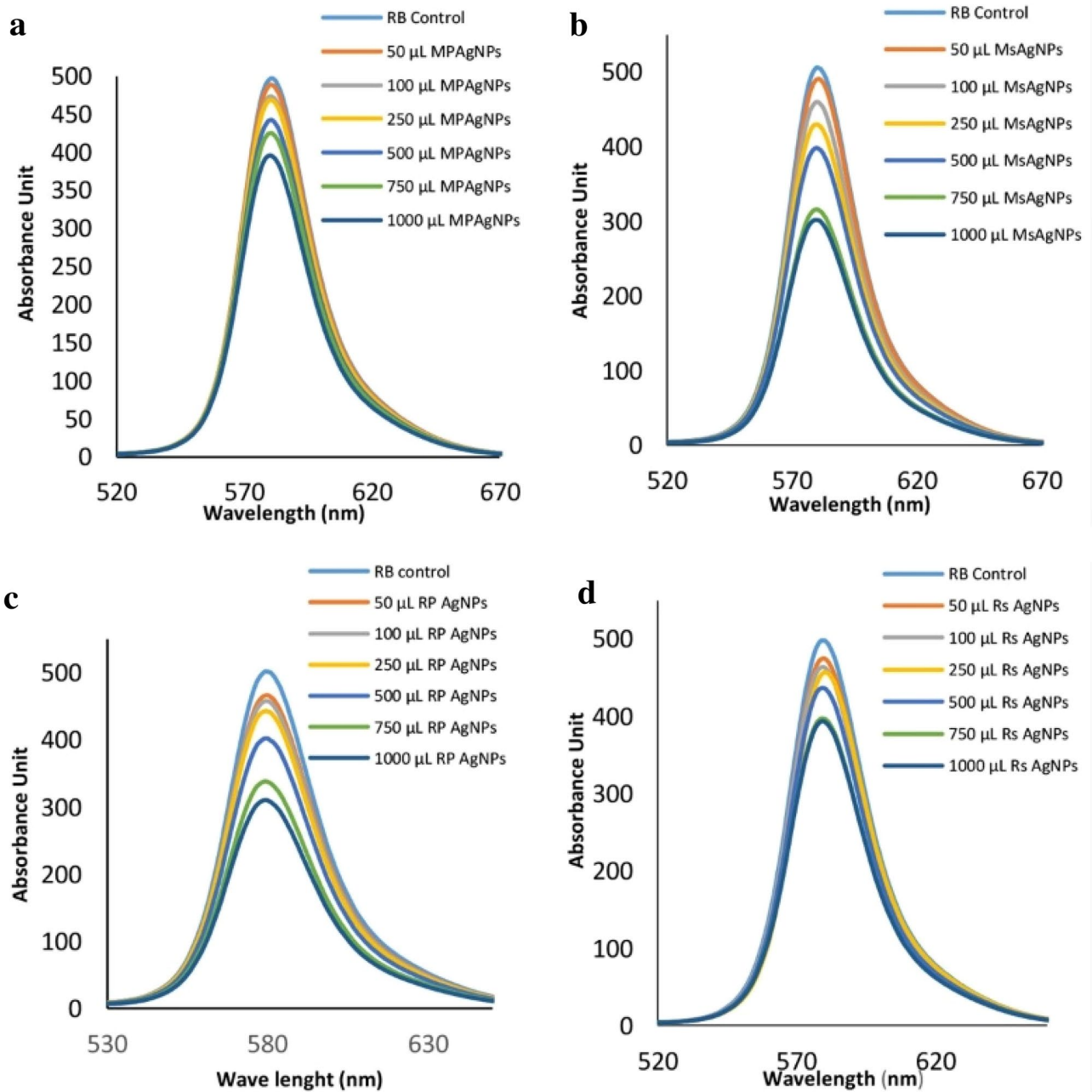


Fig. 13 Fluorescence emission spectra of Rhodamine B treated with AgNPs synthesized using **a** MPE with sunlight **b** MSE under sunlight and **c** RPE under sunlight **d** RSE under sunlight

The pH of the medium is a vital factor in the photodegradation process. The surface charge properties of the photocatalyst and the size of aggregates it forms depends on the pH. Hence, the photodegradation of the MB was carried out at pH 2, 6, and 10 to observe the effect of pH that is having on dye (without the presence of any catalyst). The experimental results revealed the higher photodegradation of MB dye in pH 10 followed by pH 6 and pH 2 as shown in Fig. 16a–c respectively. Based on the results

obtained, pH 2 was identified as a suitable pH to carry out to evaluate the photocatalytic activity of the AgNPs since the MB solution does not decompose naturally under Sunlight. To the best of the knowledge, this remains the first report wherein a study demonstrates the effect of the pH on the dye degradation using NPs. It was revealed that the MB dye was manifested insignificant degradation at pH 2 while compared with higher pH (which, therefore, could be facilitated to monitor the degradation effect of

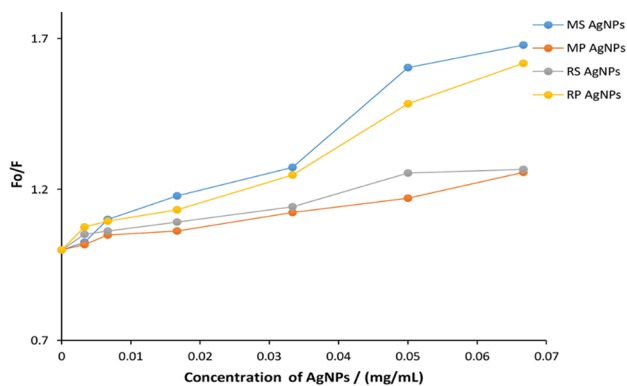


Fig. 14 Stern volmer plots obtained from the data gathered from the fluorescence emission of Rhodamine B dye treated with AgNPs of MPE (-orange), MSE (-blue), RPE (-yellow) and RSE (-blue)

the synthesized NPs without the interference of self-degradation that the dye may undergo). In most of the previous studies, it has been reported that the MB degradation was carried out at neutral or basic pH. The research carried out

by Jagdeep Singh et al. has obtained 83% MB dye degradation at 180 min (pH 7) in the presence of AgNPs.

The control (contains the AgNPs and the MB solution at pH 2), which kept under dark, did not show any degradation with time. However, the UV–VIS absorbance spectra of the MB treated with AgNPs synthesized using MPE, MSE, RPE and RSE under Sunlight demonstrated significant degradation of the dye, as shown in Fig. 17. It can be observed in Fig. 17 that the absorption intensity decreased with time considerably, within the first 30 min, in all samples. Among all the four synthesized AgNPs, rapid degradation of MB was observed in AgNPs synthesized using RSE. As per the TEM images, the AgNPs/RSE shows the highest surface area compared with the other AgNPs. This may be the reason for the rapid degradation of MB via AgNPs/RSE.

Calculation of the efficiency of the photocatalytic activities and the rate constants were performed following published literature [40]. Absorbance at the 661 nm was taken as proportional to the concentration of the MB at the determined time intervals, according to the Beer–Lambert law. The following equation was used to calculate the

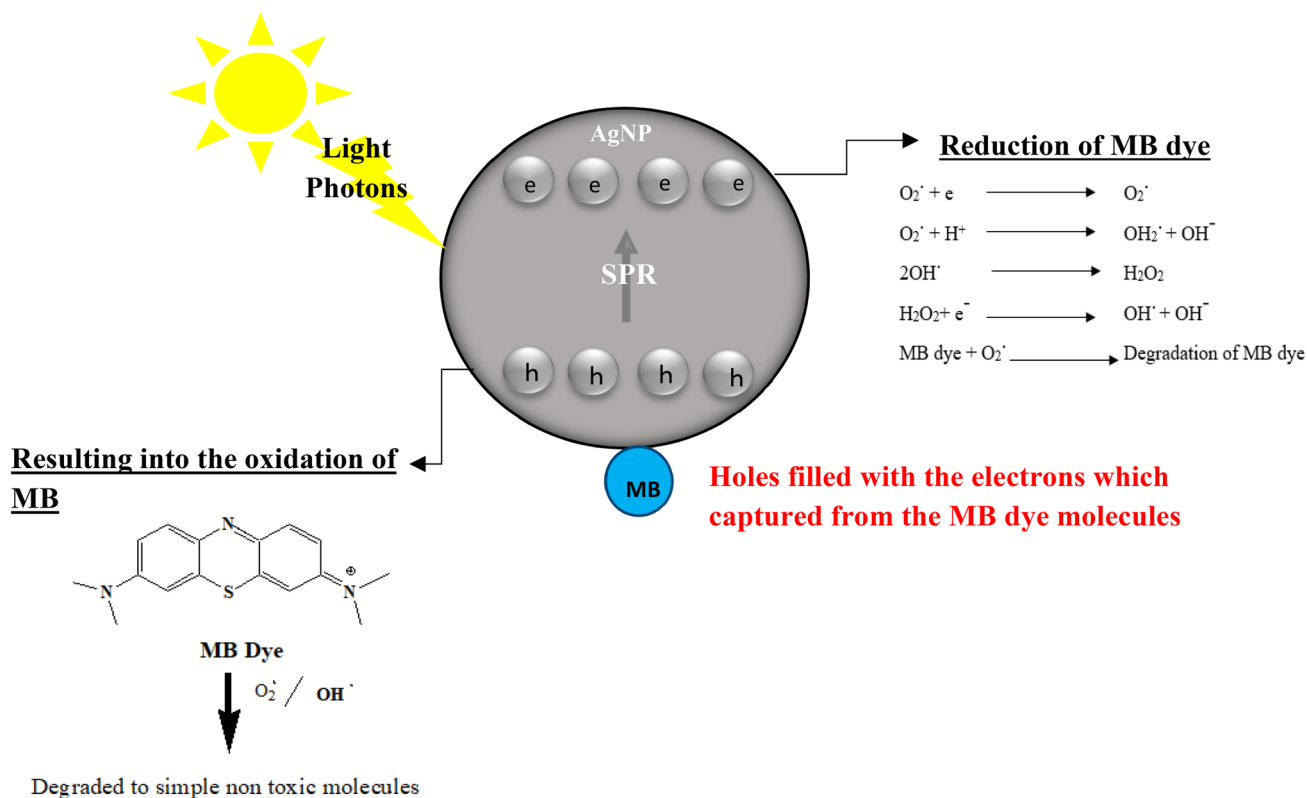


Fig. 15 Reaction mechanism of degradation of MB dye utilizing biosynthesized AgNPs. (Extracted from Singh, Jagdeep et al.)

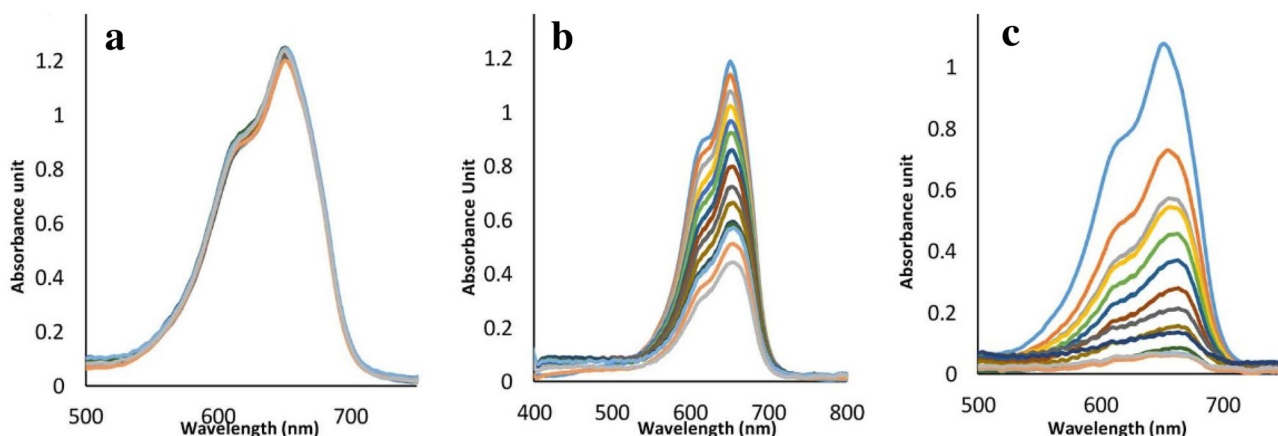


Fig. 16 UV–VIS absorbance spectra gathered for the degradation of MB dye at **a** pH 2, **b** pH 6 and **c** pH 10

degradation efficiency of the MB, where initial absorbance and absorbance at a time were denoted by C_0 and C , respectively.

$$\text{Degradation Efficiency} = \left(1 - \frac{C}{C_0}\right) \times 100\%$$

The intersection of curves [C/C_0 and $(1 - C/C_0) \times 100$] was taken as the Half-life of MB, in the presence of AgNPs [39, 70]. Degradation efficiency for each AgNPs sample were measured at 360-min time period, and plots were generated for calculating Half-life and degradation efficiencies. Information gathered on photocatalytic activity are summarized in Table 2. This study reveals that the biogenic AgNPs behave as efficient catalysts at pH 2 (360 min).

3.7.1 Adsorption isotherm study

Langmuir and Freundlich isothermal models (Figs.18, 19) were utilized to study the adsorption on MB on the sorbent surface. The figure equations are as follows:

Accordingly, with respect to the linearity of these plots, the Langmuir model is appropriate for the adsorption of MB on AgNPs. As per this model, monolayer sorption happens, and the distribution of surface-active sites of AgNPs is homogeneous.

The Langmuir isotherm follows the below equation:

$$\frac{C_e}{q_e} = \frac{1}{q_{max}b} + \frac{C_e}{q_{max}}$$

C_e —equilibrium concentration of the MB (mg/L). q_e —amount of MB adsorbed per unit mass of adsorbent (mg/g). b —maximum adsorption capacity and surface energy (the affinity between sorbent and sorbate) (mg/L).

For this study, the highest q_{max} and b were achieved as 36.76 mg/g and 0.627 mg/L for both AgNPs/MPE and AgNPs/MSE. The q_{max} observed for AgNPs/RPE and AgNPs/RSE were 17.18 mg/g and 11.81 mg/g respectively. The b constant observed for AgNPs/RPE and AgNPs/RSE were 3.10 mg/L and 1.22 mg/L respectively.

	Langmuir equation	Freundlich equation
AgNPs/MPE	$y = 0.0272x + 0.0434 (R^2 = 0.9945)$	$y = 0.5358x + 2.5536 (R^2 = 0.3305)$
AgNPs/MSE	$y = 0.0272x + 0.0434 (R^2 = 0.9945)$	$y = 0.4175x + 2.7241 (R^2 = 0.9885)$
AgNPs/RPE	$y = 0.0582x + 0.0188 (R^2 = 0.969)$	$y = 0.2718x + 2.7816 (R^2 = 0.7616)$
gNPS/RSE	$y = 0.0847x + 0.0693 (R^2 = 0.9757)$	$y = 0.5512x + 2.4945 (R^2 = 0.8036)$

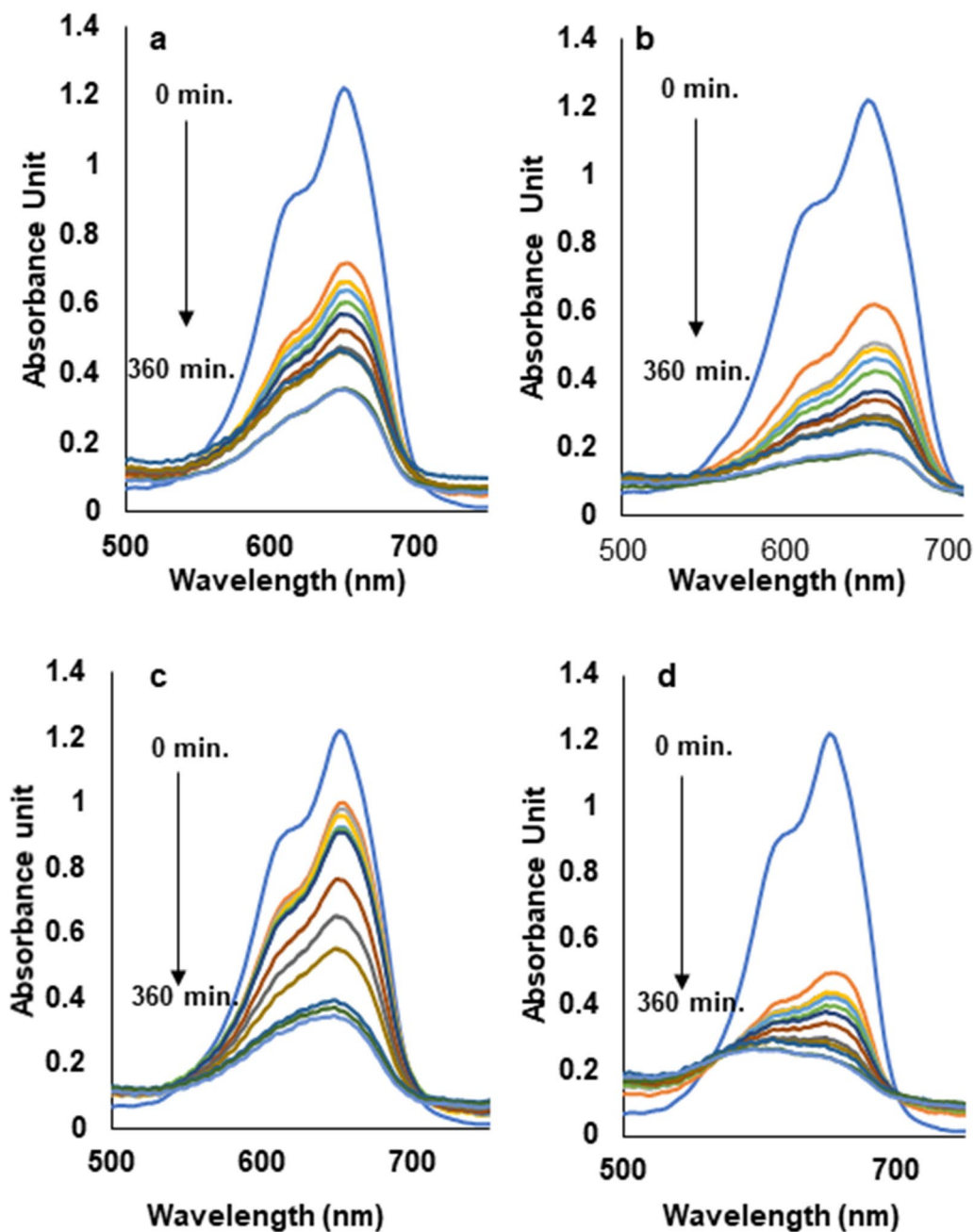


Fig. 17 Degradation of MB dye with the treatment of AgNPs synthesized via **a** MPE **b** MSE and **c** RPE **d** RSE

Table 2 Photocatalytic efficiency of the synthesized AgNPs on the degradation of MB at pH 2

AgNPs synthesized	Half-life (min)	Degradation efficiency (%)
MPE	32	78
MSE	25	91
RPE	220	82
RSE	22	95

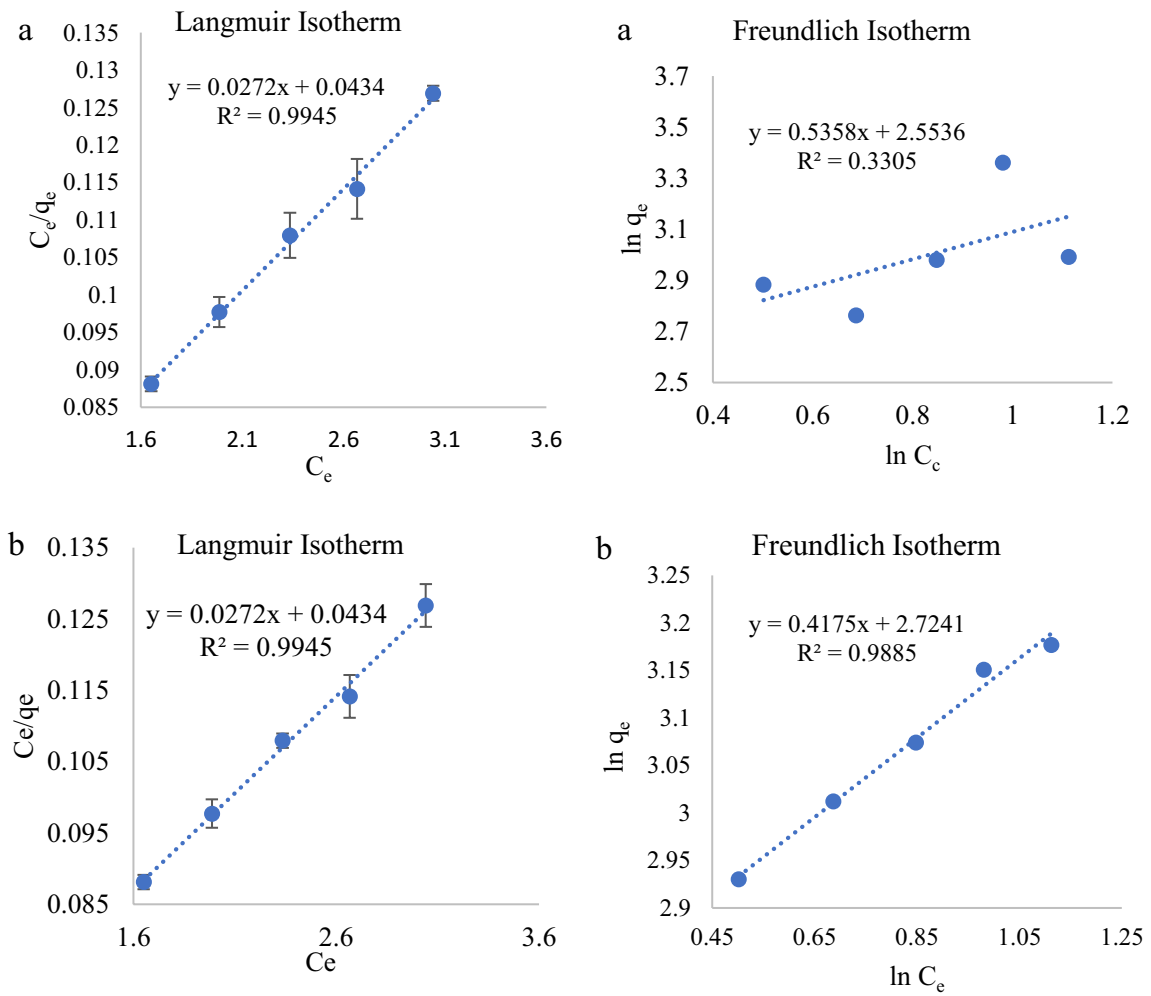


Fig. 18 Langmuir Isotherm and Freundlich Isotherm **a** MPE/AgNPs and **b** MSE/AgNPs

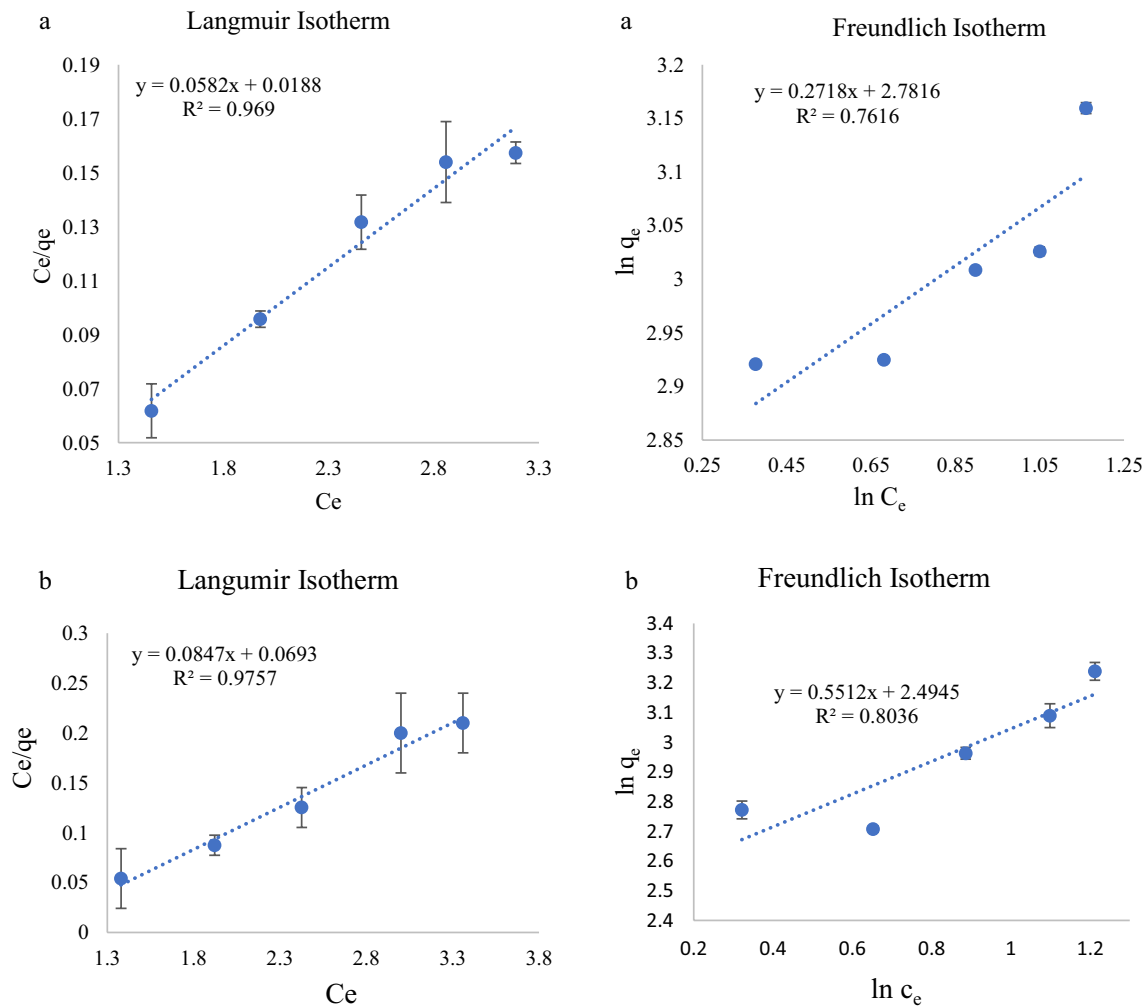


Fig. 19 Langmuir Isotherm and Freundlich Isotherm **a** RPE/AgNPs and **b** RSE/AgNPs

4 Conclusions

The results of this study suggest that the plant extracts of *G. mangostana* and *N. lappaceum* peel and seed extracts can be used as an eco-friendly reducing and capping agents in the preparation of AgNPs. The study aims at environmental sustainability through green processes to minimize agricultural wastes. The UV-Visible spectroscopic results revealed that the NPs synthesized from MPE, MSE, RPE, and RSE lie within the range of 400–440 nm and the LSPR band of green synthesized AgNPs was confirmed with the published literature. According to the SEM analysis, the NPs synthesized from MPE and RPE under direct Sunlight, and UV light was spherical with low aggregation. However, the NPs synthesized from MSE and RSE under direct Sunlight, and UV light showed higher agglomeration. The TEM analysis for all four samples reveals a nano range size distribution, which was fallen within the range

of 12.1–31.3 nm. Furthermore, the atomic interlayer distance of AgNPs synthesized via MPE, MSE, and RSE was recorded as 0.24 nm, which demonstrated the precise and uniform fringers. Considering the yield and the particle size of the AgNPs, sunlight irradiated synthesis was chosen to study the fluorescence quenching and photocatalytic activity of the NPs. To the best of our knowledge, this remains the first attempt that used biogenic AgNPs to quench the fluorescence ability of aqueous Rhodamine B solution. All the AgNPs were able to quench the fluorescence emission of Rhodamine B with increasing AgNPs concentration. The high photocatalytic activity was observed for the degradation of MB at pH 2 by all the NPs. As per the adsorption study, it was confirmed that the adsorption process is best described by the Langmuir isotherm model. The results of this study provided an ecofriendly approach to eliminate hazardous dyes from industrial effluents.

Acknowledgements The College of Chemical Sciences, Institute of Chemistry Ceylon is acknowledged for funding.

Compliance with ethical standards

Conflict of interest The author of this article declares that there is no conflict of interest regarding the publication of this paper.

References

- Adelere IA, Lateef A (2016) A novel approach to the green synthesis of metallic nanoparticles: the use of agro-wastes, enzymes, and pigments. *Nanotechnol Rev* 5(6):567–587
- Saratale RG, Karuppusamy I, Saratale GD, Pugazhendhi A, Kumar G, Park Y et al (2018) A comprehensive review on green nanomaterials using biological systems: recent perception and their future applications. *Coll Surf B Bioinform* 170:20–35
- Ahmad A, Mukherjee P, Senapati S, Mandal D, Khan MI, Kumar R et al (2003) Extracellular biosynthesis of silver nanoparticles using the fungus *Fusarium oxysporum*. *Coll Surf B Bioinform* 28(4):313–318
- Shahverdi AR, Minaeian S, Shahverdi HR, Jamalifar H, Nohi A-A (2007) Rapid synthesis of silver nanoparticles using culture supernatants of enterobacteria: a novel biological approach. *Process Biochem* 42(5):919–923
- Vijayaraghavan K, Nalini SK, Prakash NU, Madhankumar D (2012) Biomimetic synthesis of silver nanoparticles by aqueous extract of *Syzygium aromaticum*. *Mater Lett* 75:33–35
- Keerawelle BI, Chamara AMR, Thiripuranathar G (2019) A review on plant mediated synthesis of silver nanoparticles and their antimicrobial activity against various pathogenic bacteria. *J Chem Biol Phys Sci* 9(4):561–583
- Valsalam S, Agastian P, Arasu MV, Al-Dhabi NA, Ghilan A-KM, Kaviyarasu K et al (2019) Rapid biosynthesis and characterization of silver nanoparticles from the leaf extract of *Tropaeolum majus* L. and its enhanced in-vitro antibacterial, antifungal, antioxidant and anticancer properties. *J Photochem Photobiol B Biol* 191:65–74
- Lateef A, Akande MA, Azeez MA, Ojo SA, Folarin BI, Gueguim-Kana EB et al (2016) Phytosynthesis of silver nanoparticles (AgNPs) using miracle fruit plant (*Synsepalum dulcificum*) for antimicrobial, catalytic, anticoagulant, and thrombolytic applications. *Nanotechnol Rev* 5(6):507–520
- Fouda A, Abdel-Maksoud G, Abdel-Rahman MA, Salem SS, Hassan SE-D, El-Sadany MA-H (2019) Eco-friendly approach utilizing green synthesized nanoparticles for paper conservation against microbes involved in biodeterioration of archaeological manuscript. *Int Biodeterior Biodegrad* 142:160–9
- Fouda A, Abdel-Maksoud G, Abdel-Rahman MA, Eid AM, Barghoth MG, El-Sadany MA-H (2019) Monitoring the effect of biosynthesized nanoparticles against biodeterioration of cellulose-based materials by *Aspergillus niger*. *Cellulose* 26(11):6583–6597
- Alsharif SM, Salem SS, Abdel-Rahman MA, Fouda A, Eid AM, Hassan SE-D et al (2020) Multifunctional properties of spherical silver nanoparticles fabricated by different microbial taxa. *Heliyon* 6(5):e03943
- Adebayo EA, Ibikunle JB, Oke AM, Lateef A, Azeez MA, Oluwatoyin AO, AyanfeOluwa AV, Blessing OT, Comfort OO, Adekunle OO, Badmus JA (2019) Antimicrobial and antioxidant activity of Silver, Gold and Silver-Gold Alloy Nanoparticles phytosynthesized using extract of *Opuntia ficus-indica*. *Rev Adv Mater Sci* 58(1):313–326
- Raagulan K, Mantilaka MM, Chandrakumara G, Ekanayake UM, Wijesinghe W, Ehanathan S et al (2019) Sunlight active $U_3O_8@ZnO$ nanocomposite superfast photocatalyst: synthesis, characterization and application. *Nanoscale Adv* 1(2):481–485
- Lateef A, Ojo SA, Elegbede JA, Akinola PO, Akanni EO (2018) Nanomedical applications of nanoparticles for blood coagulation disorders. *Environ Nanotechnol* 14:243–277
- Adebayo AE, Oke AM, Lateef A, Oyatokun AA, Abisoye OD, Adiji IP et al (2019) Biosynthesis of silver, gold and silver-gold alloy nanoparticles using *Persea americana* fruit peel aqueous extract for their biomedical properties. *Nanotechnol Environ Eng* 4(1):13
- Lateef A, Azeez MA, Asafa TB, Yekeen TA, Akinboro A, Oladipo IC et al (2016a) Biogenic synthesis of silver nanoparticles using a pod extract of *Cola nitida*: antibacterial and antioxidant activities and application as a paint additive. *J Taibah Univ Sci* 10(4):551–562
- Lateef A, Azeez MA, Asafa TB, Yekeen TA, Akinboro A, Oladipo IC et al (2016b) Cocoa pod husk extract-mediated biosynthesis of silver nanoparticles: its antimicrobial, antioxidant and larvicidal activities. *J Nanostructure Chem* 6(2):159–169
- Saratale RG, Saratale GD, Shin HS, Jacob JM, Pugazhendhi A, Bhisare M et al (2018) New insights on the green synthesis of metallic nanoparticles using plant and waste biomaterials: current knowledge, their agricultural and environmental applications. *Environ Sci Pollut Res* 25(11):10164–10183
- Kumar B, Smita K, Cumbal L, Angulo Y (2015) Fabrication of silver nanoplates using *Nephelium lappaceum* (Rambutan) peel: a sustainable approach. *J Mol Liq* 211:476–480
- Pedraza-Chaverri J, Cárdenas-Rodríguez N, Orozco-Ibarra M, Pérez-Rojas JM (2008) Medicinal properties of mangosteen (*Garcinia mangostana*). *Food Chem Toxicol* 46(10):3227–3239
- Ming-Hui W, Zhang K-J, Qin-Lan G, Xiao-Ling B, Jin-Xin W (2017) Pharmacology of mangostins and their derivatives: a comprehensive review. *Chin J Nat Med* 15(2):81–93
- Mahmood K, Kamilah H, Alias AK, Ariffin F (2018) Nutritional and therapeutic potentials of rambutan fruit (*Nephelium lappaceum* L.) and the by-products: a review. *J Food Meas Charact* 12(3):1556–1571
- Sukmandari NS, Dash G, Jusof WHW, Hanafi M (2017) A review on *Nephelium lappaceum* L. *Res J Pharm Technol* 10:2819–2827
- Uduwela UDHK, Deraniyagala SA, Thiripuranathar G (2019) Antioxidant and anti-inflammatory potential of the aqueous extract of the peel of a sri lankan variety of *nephelium lappaceum* linn. *World J Pharma Res* 8(2):154–166
- Lateef A, Folarin BI, Oladejo SM, Akinola PO, Beukes LS, Gueguim-Kana EB (2018) Characterization antimicrobial antioxidant and anticoagulant activities of silver nanoparticles synthesized from *Petiveria alliacea* L. leaf extract. *Prep Biochem Biotechnol* 48(7):646–652
- Elango G, Roopan SM (2016) Efficacy of SnO_2 nanoparticles toward photocatalytic degradation of methylene blue dye. *J Photochem Photobiol B Biol* 155:34–38
- Saratale GD, Saratale RG, Chang JS, Govindwar SP (2011) Fixed-bed decolorization of reactive blue 172 by *Proteus vulgaris* NCIM-2027 immobilized on *Luffa cylindrica* sponge. *Int Biodeterior Biodegrad* 65(3):494–503
- Elfeky AS, Salem SS, Elzaref AS, Owda ME, Eladawy HA, Saeed AM et al (2020) Multifunctional cellulose nanocrystal/metal oxide hybrid, photo-degradation, antibacterial and larvicidal activities. *Carbohydr Polym* 230:115711
- Saratale GD, Saratale RG, Cho S-K, Ghodake G, Bharagava RN, Park Y et al (2020) Investigation of photocatalytic degradation of reactive textile dyes by *Portulaca oleracea*-functionalized silver nanocomposites and exploration of their antibacterial and antidiabetic potentials. *J Alloy Compd* 833:155083

30. Saratale RG, Ghodake GS, Shinde SK, Cho S-K, Saratale GD, Pugazhendhi A et al (2018) Photocatalytic activity of CuO/Cu(OH)₂ nanostructures in the degradation of reactive green 19A and textile effluent, phytotoxicity studies and their biogenic properties (antibacterial and anticancer). *J Environ Manag* 223:1086–1097
31. Tkaczyk A, Mitrowska K, Posyniak A (2020) Synthetic organic dyes as contaminants of the aquatic environment and their implications for ecosystems: a review. *Sci Total Environ* 717:137222
32. Jiang K, Pinchuk AO (2015) Noble metal nanomaterials: synthetic routes, fundamental properties, and promising applications. *Solid State Phys* 66:131–211
33. Vijaya JJ, Jayaprakash N, Kombaiah K, Kaviyarasu K, Kennedy LJ, Ramalingam RJ et al (2017) Bioreduction potentials of dried root of *Zingiber officinale* for a simple green synthesis of silver nanoparticles: antibacterial studies. *J Photochem Photobiol B Biol* 177:62–68
34. Gogoi N, Babu PJ, Mahanta C, Bora U (2015) Green synthesis and characterization of silver nanoparticles using alcoholic flower extract of *Nyctanthes arbortristis* and in vitro investigation of their antibacterial and cytotoxic activities. *Mater Sci Eng C* 46:463–469
35. Parveen M, Ahmad F, Malla AM, Azaz S (2016) Microwave-assisted green synthesis of silver nanoparticles from *Fraxinus excelsior* leaf extract and its antioxidant assay. *Appl Nanosci* 6(2):267–276
36. Kumar B, Smita K, Cumbal L, Debut A (2017) Sacha inchi (*Plukenetia volubilis* L.) shell biomass for synthesis of silver nanocatalyst. *J Saudi Chem Soc* 21:293–298
37. Tade RS, Nangare SN, Patil PO (2020) Agro-industrial waste-mediated green synthesis of silver nanoparticles and evaluation of its antibacterial activity. *Nano Biomed Eng* 12(1):57–66
38. Keerawelle BI, Chamara AMR, Thiripuranathar G (2019) Green synthesis of silver nanoparticles via medicinal plant extracts and their antibacterial activities. *World J Pharm Res* 8(7):100–111
39. Kuruppu KASS, Perera KMK, Chamara AMR, Thiripuranathar G (2020) Flower shaped ZnO—NPs; phytofabrication, photocatalytic, fluorescence quenching, and photoluminescence activities. *Nano Express* 1(2):020020
40. Panchompoo J, Aldous L, Baker M, Wallace MI, Compton RG (2012) One-step synthesis of fluorescein modified nano-carbon for Pd(II) detection via fluorescence quenching. *The Analyst* 137(9):2054–2062
41. Rashad MM, Ismail AA, Osama I, Ibrahim I, Kandil A-HT (2014) Photocatalytic decomposition of dyes using ZnO doped SnO₂ nanoparticles prepared by solvothermal method. *Arab J Chem* 7(1):71–77
42. Ravindran A, Singh A, Raichur AM, Chandrasekaran N, Mukherjee A (2010) Studies on interaction of colloidal Ag nanoparticles with bovine serum albumin (BSA). *Coll Surf B Bioinform* 76(1):32–37
43. Kakhki RM, Hedayat S, Mohammadzadeh K (2019) Novel, green and low cost synthesis of Ag nanoparticles with superior adsorption and solar based photocatalytic activity. *J Mater Sci Mater Electron* 30(9):8788–8795
44. Darroudi M, Ahmad MB, Zak AK, Zamiri R, Hakimi M (2011) Fabrication and characterization of gelatin stabilized silver nanoparticles under UV-light. *Int J Mol Sci* 12(9):6346–6356
45. Anand K, Kaviyarasu K, Muniyasamy S, Roopan SM, Gengan R, Chuturgoon A (2017) Bio-synthesis of silver nanoparticles using agroforestry residue and their catalytic degradation for sustainable waste management. *J Clust Sci* 28(4):2279–2291
46. Thomas B, Vithiya B, Prasad T, Mohamed S, Magdalane CM, Kaviyarasu K et al (2019) Antioxidant and photocatalytic activity of aqueous leaf extract mediated green synthesis of silver nanoparticles using *Passiflora edulis* f. flavicarpa. *J Nanosci Nanotechnol* 19(5):2640–2648
47. Thangaraju N, Venkatalakshmi R, Chinnasamy A, Kannaiyan P (2012) Synthesis of silver nanoparticles and the antibacterial and anticancer activities of the crude extract of *Sargassum polycystum* C. Agardh. *Nano Biomed Eng* 4(2):89–94
48. Behravan M, Panahi AH, Naghizadeh A, Ziaee M, Mahdavi R, Mirzapour A (2019) Facile green synthesis of silver nanoparticles using *Berberis vulgaris* leaf and root aqueous extract and its antibacterial activity. *Int J Biol Macromol* 124:148–154
49. Rautela A, Rani J, Das MD (2019) Green synthesis of silver nanoparticles from *Tectona grandis* seeds extract: characterization and mechanism of antimicrobial action on different microorganisms. *J Anal Sci Technol* 10(1):1–10
50. Cakić M, Glišić S, Cvetković N, Stanojević L, Danilović B et al (2018) Green synthesis, characterization and antimicrobial activity of silver nanoparticles produced from *Fumaria officinalis* L. *Plant Extr Colloid J* 80(6):803–813
51. Park JS, Ahn E-Y, Park Y (2017) Asymmetric dumbbell-shaped silver nanoparticles and spherical gold nanoparticles green-synthesized by mangosteen (*Garcinia mangostana*) pericarp waste extracts. *Int J Nanomed* 12:6895
52. Lestari P, Pratiwi I, Juliani A editors (2018) Green synthesis of silver nanoparticle using rambutan (*Nephelium lappaceum* L.) peel extract and its antibacterial activity against *Salmonella paratyphi* A. In: MATEC web of conferences EDP sciences. 154
53. Horikoshi S, Serpone N (2013) Introduction to nanoparticles. In: Serpone N, Horikoshi S (eds) *Microwaves in nanoparticle synthesis: fundamentals and applications*. Wiley, Weinheim, pp 1–24
54. Manimekalai I, Sivakumari K, Ashok K, Rajesh S (2016) Phytochemical profiling of mangosteen fruit, *Garcinia mangostana*. *World J Pharm Pharm Sci* 5(2):221–252
55. Chai KF, Mohd Adzahan N, Karim R, Rukayadi Y, Ghazali HM (2018) Characteristics of fat, and saponin and tannin contents of 11 varieties of rambutan (*Nephelium lappaceum* L.) seed. *Int J Food Prop* 21(1):1091–1106
56. Verma DK, Hasan SH, Banik RM (2016) Photo-catalyzed and phyto-mediated rapid green synthesis of silver nanoparticles using herbal extract of *Salvinia molesta* and its antimicrobial efficacy. *J Photochem Photobiol B Biol* 155:51–59
57. Kumar V, Gundampati RK, Singh DK, Jagannadham MV, Sundar S, Hasan SH (2016) Photo-induced rapid biosynthesis of silver nanoparticle using aqueous extract of *Xanthium strumarium* and its antibacterial and antileishmanial activity. *J Ind Eng Chem* 37:224–236
58. Jayaprakash N, Vijaya JJ, Kaviyarasu K, Kombaiah K, Kennedy LJ, Ramalingam RJ et al (2017) Green synthesis of Ag nanoparticles using tamarind fruit extract for the antibacterial studies. *J Photochem Photobiol B Biol* 169:178–185
59. Fouda A, Hassan SE-D, Abdo AM, El-Gamal MS (2019) Antimicrobial, antioxidant and larvicidal activities of spherical silver nanoparticles synthesized by endophytic *Streptomyces* spp. *Biol Trace Elem Res* 195(2):1–18
60. Soliman AM, Abdel-Latif W, Shehata IH, Fouda A, Abdo AM, Ahmed YM (2020) Green approach to overcome the resistance pattern of *Candida* spp. using biosynthesized silver nanoparticles fabricated by *Penicillium chrysogenum* F9. *Biol Trace Elem Res*. <https://doi.org/10.1007/s12011-020-02188-7>
61. Khan MAM, Kumar S, Ahamed M, Alrokayan SA, AlSalhi MS (2011) Structural and thermal studies of silver nanoparticles and electrical transport study of their thin films. *Nanoscale Res Lett* 6(1):434
62. Mohamed AA, Fouda A, Elgamal MS, El-Din Hassan S, Shaheen TI, Salem SS (2017) Enhancing of cotton fabric antibacterial properties by silver nanoparticles synthesized by new Egyptian strain *Fusarium keratoplasticum*. *Egypt J Chem* 60:63–71

63. Lateef A, Ojo SA, Elegbede JA (2016) The emerging roles of arthropods and their metabolites in the green synthesis of metallic nanoparticles. *Nanotechnol Rev* 5(6):601
64. Bardajee GR, Hooshyar Z, Khanjari M (2014) Dye fluorescence quenching by newly synthesized silver nanoparticles. *J Photochem Photobiol A Chem* 276:113–121
65. Castillo JJ, Cano H (2017) Study of the fluorescence quenching of 1-hydroxypyrene-3, 6, 8-trisulfonic acid by single-walled carbon nanotubes. *Univ Sci* 22(3):201–214
66. Jesudoss S, Vijaya JJ, Rajan PI, Kaviyarasu K, Sivachidambaram M, Kennedy LJ et al (2017) High performance multifunctional green Co_3O_4 spinel nanoparticles: photodegradation of textile dye effluents, catalytic hydrogenation of nitro-aromatics and antibacterial potential. *Photochem Photobiol Sci* 16(5):766–778
67. Salem SS, Fouda A (2020) Green synthesis of metallic nanoparticles and their prospective biotechnological applications: an overview. *Biol Trace Elem Res.* <https://doi.org/10.1007/s12011-020-02138-3>
68. Singh J, Dhaliwal A (2020) Plasmon-induced photocatalytic degradation of methylene blue dye using biosynthesized silver nanoparticles as photocatalyst. *Environ Technol* 41(12):1520–1534
69. Chen X, Zheng Z, Ke X, Jaatinen E, Xie T, Wang D et al (2010) Supported silver nanoparticles as photocatalysts under ultraviolet and visible light irradiation. *Green Chem* 12(3):414–419
70. Soltani N, Saion E, Hussein MZ, Erfani M, Abedini A, Bahmanrokh G et al (2012) Visible light-induced degradation of methylene blue in the presence of photocatalytic ZnS and CdS nanoparticles. *Int J Mol Sci* 13(10):12242–12258

Publisher's Note Springer Nature remains neutral with regard to jurisdictional claims in published maps and institutional affiliations.